A Review on Structural Fire Tests of Two-Way Composite Floors

Mhd Anwar Orabi, Liming Jiang*, Xinyan Huang*, Asif Usmani

Research Centre for Fire Safety Engineering, Department of Building Environment and Energy Engineering, The Hong Kong Polytechnic University, Hong Kong

* Correspondence to liming.jiang@polyu.edu.hk; xy.huang@polyu.edu.hk

Abstract: The utilisation of composite floor systems in modern construction allows for building large floor areas with efficient use of material and labour. The efficiency of this flooring system in carrying ambient loads as well as the thermal thinness of its steel framing makes it hypothetically sensitive to fire loads as a small exposure time may result in a rapid increase in temperature. However, a series of fire events and then large-scale experiments at the turn of the century demonstrated that composite floors could display surprising robustness in the face of high temperatures. Soon after, the total collapse of the World Trade Center towers 1, 2 and 7 showed the opposite. For the two decades since then, a large amount of experimental and theoretical work has been performed on this topic. This review aims to formulate an understanding of the thermo-mechanical behaviour of composite floors in fire, and to leverage that understanding to design more efficient and more robust buildings. We first surveyed the literature, and then summarized the composite floors being studied into three categories: isolated composite slab panels, composite floor assemblies, and large-scale tests. Then, theoretical design and analysis methods are discussed in light of the reviewed literature. Finally, this review coalesces the knowledge generated from the literature and lists the remaining challenges in the area, and set out a set of recommendations for designing composite floor systems for fire.

Keywords: *slab; steel construction; tall buildings; structure fire design; tensile membrane action.*

Graphic Abstract

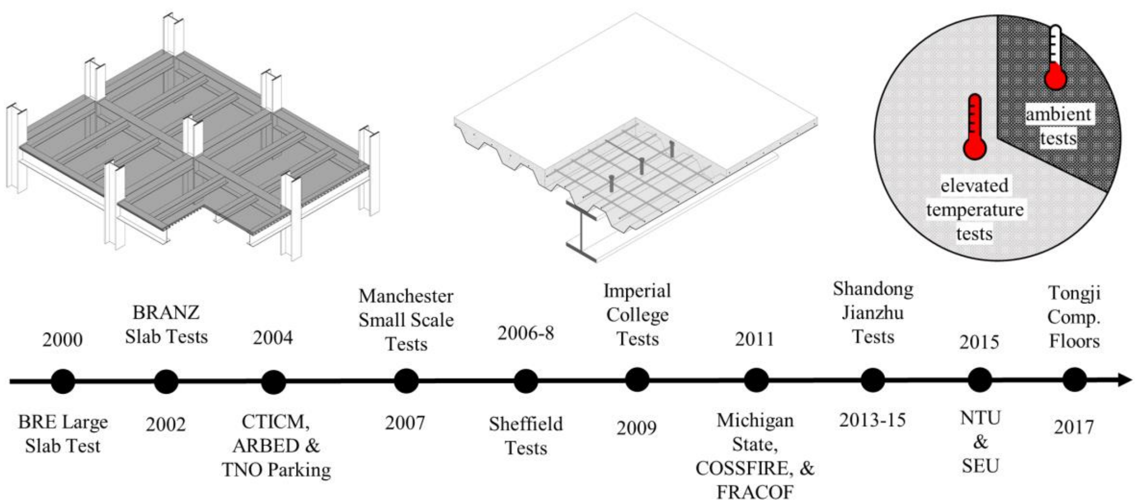

1. Introduction

1.1. Composite Floor Construction

Composite construction generally utilises steel framing in combination with a steel-concrete composite floor slab. This form of construction allows for fast erection times due to the relatively straight-forward assembly of well-designed prefabricated steel sections and connections. Once floor framing is assembled, the floor slab can be cast-in-place directly atop the steel profiled sheeting that will act as its bottom reinforcement. This kind of construction has become ubiquitous in modern buildings for many reasons such as its low weight-to-stiffness ratio, forgiving tolerances, and exceptional speed at which construction can proceed. The manufacturers of the steel sheeting over which the concrete of the composite floor is poured produce standardized steel-decking profiles with a typical thickness of 0.8 – 1.2 mm. These profiles are supplied with thorough documentation on required concrete thickness for different service and ultimate loads as well as information on requirements to achieve specified fire ratings.

An 'anti-cracking' steel mesh is placed within the continuous portion above the ribs, with a prescribed minimum reinforcement of 80 mm^2/m in each direction as per the EN 1994-1-1 [1]. For the edges of the slab where hogging moments are expected, the minimum cracking steel area above the ribs is also bound by being no less than 0.2% - 0.4% for propped and unpropped construction, respectively. This mesh serves to reduce cracking that may occur as concrete cures and shrinks and is not meant to act as primary flexural reinforcement under normal conditions, which is a task for the steel decking. During construction, the steel sheeting is placed on top of the steel frame and shot-fired onto the floor beams, before shear connectors are welded on, steel mesh placed, and concrete poured resulting in the arrangement shown in Fig. 1(a). Various types of shear connectors are used in construction but headed shear studs placed in individual or paired sets are the most common in composite buildings [2]. The composite floor slab is often designed as a set of connected panels with one or more secondary beams bridging the gap between two primary beams as seen in Fig. 1(b), with the ribs of the slab running perpendicular to the secondary beams.

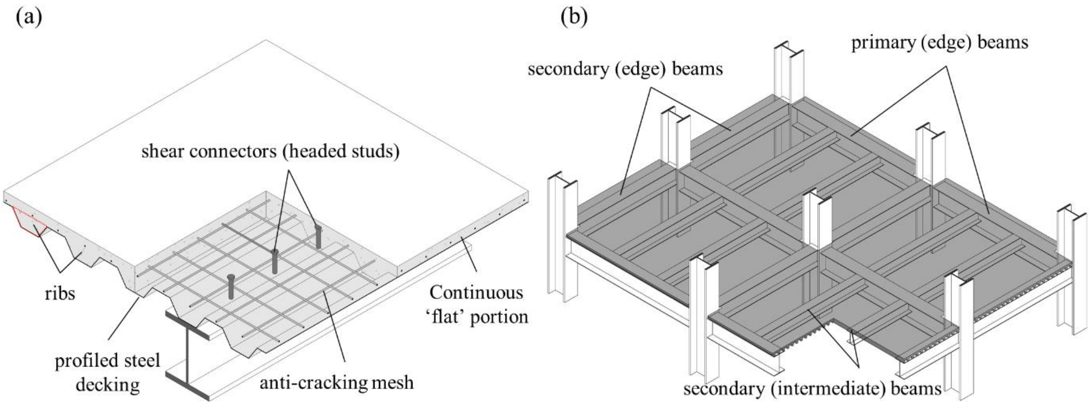

Fig. 1. Composite floor construction (a) components of a composite slab connected to a beam with shear studs, and (b) composite floor construction with two intermediate beams supporting the slab panel.

1.2. Fire Resistance of Composite Floor Construction

It has become increasingly common to design some secondary members without fire protection since the observation of excess capacity in fire after Broadgate Phase 8 fire incident and the Cardington tests [3–5]. The Broadgate Phase 8 fire incident had shown that composite floors subject to uncontrollable fire exposure may deflect severely but remain structurally intact. The Cardington tests were then performed to cross-check this phenomenon and indeed confirmed that composite structures may possess exceptional fire robustness. Thus, instead of protecting all members, composite floor systems are designed as a set of panels where the intermediate beams are left unprotected while the perimeter primary and secondary beams as well as all columns are protected [6]. Intermediate beams are those that cross the span of the slab panel between two primary or secondary beams as shown in Fig. 1 (b). The rationale behind protecting the perimeter beams from fire but leaving the internal beams bare emerged from the observation of the mechanism in which composite floors redistribute thermal loads. After the Broadgate fire which lasted for four and a half hours, it was observed clearly that the floor had achieved deflections orders of magnitude above those achieved under regular conditions. The structure avoided collapse but was irreparable.

The Cardington series of fire tests performed in the middle 1990s reiterated this observation, with floor deflections reaching up to $L/15$ where L is the span of the secondary beams (9 m). The fires used to stress the structure during the Cardington tests were realistically severe and reasonably timed to between 1.5 to 2 hours, but the full-scale Cardington test building showed no signs of global or localised collapse after all seven tests were performed. The insights from the Cardington experiment advanced the state of the art regarding the behaviour of steel-framed construction in fire and helped set the foundations for the use of tensile membrane action (TMA) to explain the robustness of composite floors in fire. At ambient, composite floors resist applied load by one way bending because of the high length to width ratio of the slab panels supported on the intermediate beams as shown in Fig. 1 (b). In fire, intermediate beams lose their capacity and restrained thermal expansion of the slab is relieved by adopting large deflections. This leads to the development of tensile membrane forces acting in both in-plane directions that enable the floor to resist the fire [7, 8]. This behaviour is what referred to in this paper as two-way action.

Understanding the phenomenon of TMA and harnessing it for structural design has been one of two primary aims for a significant number of experimental research projects carried out over the last two decades. The other primary aim for research on the behaviour of composite floors came about from the collapse of the World Trade Center towers 1, 2, and 7 and is concerned with pinpointing the failure mechanisms responsible for the collapse of composite floor systems. The 11 September 2001 disaster showcased to the structural engineering community how fire could cause code-compliant construction to collapse in a matter of a few hours. All three collapsed buildings were steel framed, and the collapse of World Trade Center 7 remains the most puzzling with expert investigations pointing to different causes for its failure most of which originate in the composite floor and its connections [9, 10]. The experimental work performed over the last two decades provides important insight into how composite floor systems resist fire, how fire damages these systems, and failure of composite floors initiates.

In this review, structural fire tests on composite floor systems can be divided into three categories based on scale and test conditions: 1. Isolated composite slab panels, 2. Composite floor assemblies, and 3. Large scale system-level tests. An isolated panel refers to tests performed only on the slab-portion of the composite floor with idealised boundary conditions enforced by testing setup. Composite floor assemblies include part of the steel framing such as primary and secondary beams that would be an integral part of typical composite construction. A large-scale system-level test refers to experiments performed on a complete composite building such as the Cardington tests.

Each test will be discussed in detail starting with thorough description of the specimens, boundary conditions enforced, and mechanical and thermal load applied. The results summarised will include the temperature distribution, deflections achieved, and damage pattern and failure mode if any. These experimentally observable aspects of the behaviour cover the majority of concerns structural engineers may have regarding the behaviour of composite slabs both locally and as part of a larger structure. The literature reviewed is limited to work published since 2000, as research before then has been reviewed in [11–13].

Since large deflections are a fundamental aspect of the response of composite floors in fire, some early tests aimed to simulate the fire behaviour of composite slabs by inducing large central deflections at ambient conditions. The rationale behind these tests was that large deflections, regardless of how they were induced, would result in a TMA mechanism, and may provide insight on the possible large-deflection behaviour and failure modes. These tests were fundamental in bringing the state of the art to the stage at which it is today and form the background for many of the theoretical models used for analysing and designing composite floors in fire. Therefore, tests that were performed at ambient conditions in order to study fire resistance of composite slabs are included in this review.

Tests on isolated composite beams are not included in this review because this paper is concerned with two-way action of composite floors rather than the behaviour of individual beams. Likewise, tests on slabs with non-traditional reinforcement such as steel fibres are outside the scope of this review and so are composite construction utilising steel beams cast within the slab (*Slimflor* construction) or construction on special forms of floor framing such as cellular beams [14, 15]. The tests covered in this review as well as their defining characteristic (i.e. ambient vs. elevated temperature test, ribbed vs. flat slab, and isolated vs. assembly vs. large-scale) are shown in Fig. 2. The experimental work shown in the figure are dated according to their publication either in a technical report [16, 17], a PhD thesis [18, 19], or a journal article [20, 21]. Overall, there were 133 tests, out of which 90 were performed at elevated temperatures and the rest at ambient. Of the tests that were carried out, 109 were performed on isolated slab specimens with simplified boundary conditions, 18 on assemblies including a slab composite with floor framing, and 6 were performed on a full structure.

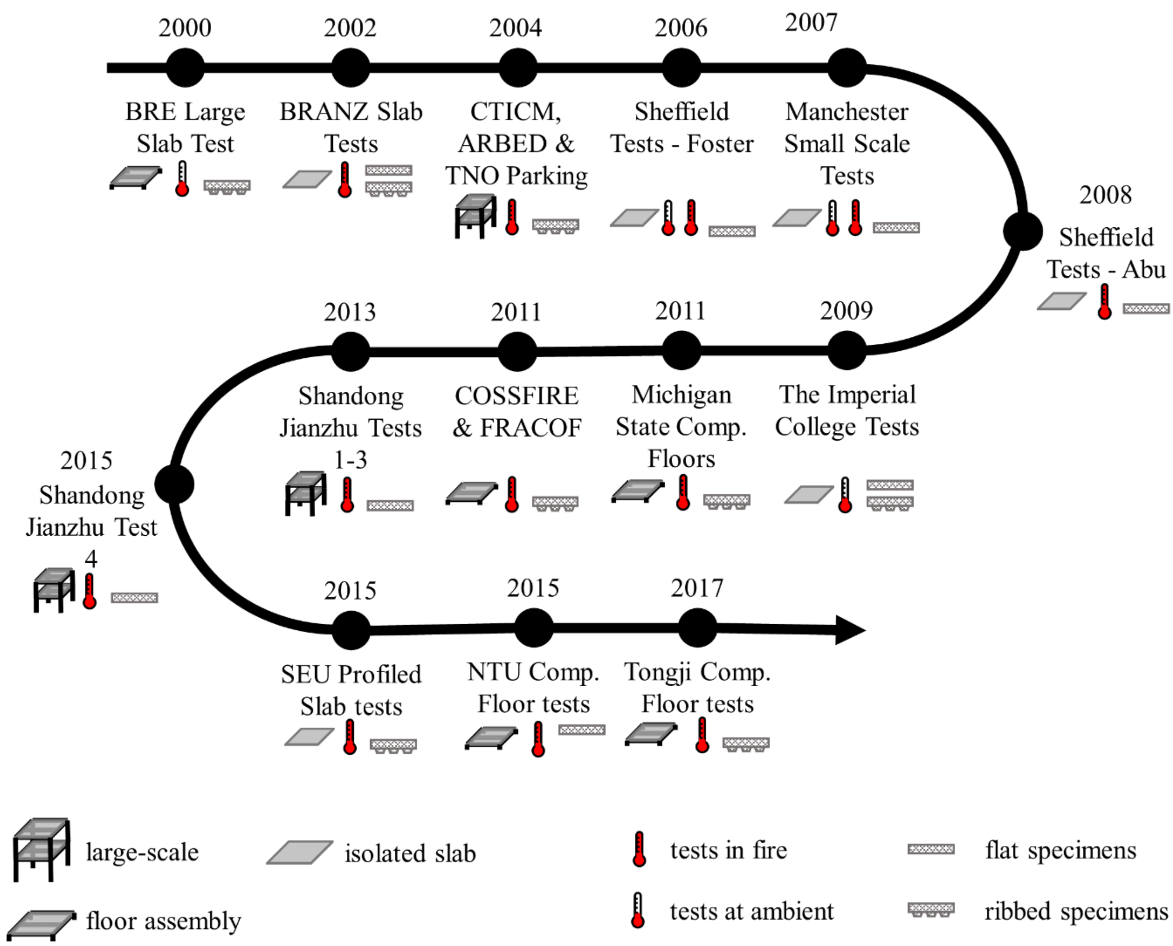

Fig. 2. Timeline and characteristics of the tests covered in this review based on publication date

The last section of this paper will give an overview of the theoretical approaches for designing and analysing composite floors in fire. These methods underwent rapid development since the early 2000's with the emergence of Bailey's yield line approach [22]. Many theoretical approaches after it inherited its fundamental ideas and modified different aspects of it to either expand its scope or overcome its shortcomings. After the overview of the theoretical approaches, this paper summarises the observed failure and damage mechanisms in the tests, and then pinpoints the gaps in the existing body of knowledge for future research. Finally, important considerations for practice concerning the design and analysis of composite floor systems in fire are highlighted.

The authors acknowledge, from first-hand experience, that performing structural fire experiments is an exceedingly costly, laborious, and relatively risky endeavour. During this review, the authors may remark on the effects of some assumptions made in the literature or re-interpret some experimental results. This is done to maximize the utility of the performed experiments and build upon the theoretical understanding developed by previous researchers. The discussion made within this paper is not meant to unduly criticize or belittle the tremendous efforts and valuable findings of those who have paved the way for the field to reach its current state of the art.

2. Tests on Isolated Composite Slab Panels

Tests on isolated panels consider the slab disjoint from any floor beams and are performed mostly on simplified boundary conditions. This kind of experiment presuppose two primary conditions: (1) Intermediate beams are unprotected and lose all capacity shortly after the fire, and (2) Vertical edge support will always be provided by the adjacent ‘cold’ structure. With these assumptions established, the performance of the individual panels are considered to hold as a representation of the most basic component of the two-way floor system, and its failure marking the critical limit state of the floor.

2.1. BRANZ Slab Tests

Lim and Wade [23] performed a series of six full-scale elevated temperature tests on simply supported reinforced concrete, composite concrete on steel deck, and special construction specimens. The testing was performed at the Building Research Association of New Zealand (BRANZ) and published in a technical report in 2002 [23]. All specimens had a rectangular footprint of 3.3 m × 4.3 m but were varied in thickness depending on their type. The flat slabs had a thickness of 100 mm, while the ribbed ‘Hi-bond’ specimen had a total depth of 130 mm with 55 mm deep ribs. The ‘Traydec’ slab used flat steel sheeting and had a total thickness of 130 mm. The last slab, Speedfloor, was constructed to be composite with 3 mm thick steel joists and thus falls outside the scope of this paper. In all specimens, the reinforcement in the short direction was placed below the long direction rebars, while the ribs and joists of the Hibond slab were along the long span. Details of the various specimens are presented in Table 1.

Table 1. Specifications of test specimens for the BRANZ fire tests [23, 24]

Specimen	**Thickness**	**Reinforcement type**	**Reinforcement area**	**Rebar yield strength**	**Steel deck**	**Deck yield strength**	**Concrete cover**
661	100 mm	Cold-drawn plain mesh	295 mm^2/m	568 MPa	_	_	25 mm
D147	100 mm	Cold-drawn deformed mesh	198 mm^2/m	565 MPa	_	_	25 mm
HD12	100 mm	Hot-rolled deformed bars	565 mm^2/m	468 MPa	_	_	25 mm
Hibond	130 mm	Cold-drawn deformed mesh	198 mm^2/m	565 MPa	0.75 mm	550 MPa	20 mm
Traydec	130 mm	Cold-drawn deformed mesh	198 mm^2/m	565 MPa	0.75 mm	550 MPa	15 mm
Speedfloor	90 mm	Cold-drawn plain mesh	300 mm^2/m	568 MPa	3.0 mm	350 MPa	25 mm

All specimens were unrestrained laterally and rotationally at their edges. This low level of restraint resulted in the corners of the flat specimens 661 and HD12 curling upwards due to thermal gradient and thus diverge from the intended support conditions. Specimen D147 and the remaining composite slabs were tested with steel clamps holding their corners down. A unique hydrostatic loading apparatus was used to apply a uniformly distributed live load to the slabs with a magnitude of 3 kN/m^2, in addition to the self-weight of the specimens. The total load including the self-weight of the specimens varied between 5.31 kN/m^2 up to 6.02 kN/m^2. All specimens were subjected to the ISO 834 temperature-time curve for up to three hours. Thermocouple trees, strain gauges, and rotary potentiometers were used to measure the experimental temperatures, strains, and deflections respectively.

The maximum temperatures reached in the rebars in the flat slabs were between 700 °C and 800 °C. In the Hibond slab, the temperature was measured in the reinforcement within the thin continuous portion and the rebars above the ribs. The rebars located above the ribs showed temperatures that are about 200 °C lower than the temperatures in the thin continuous portion of the slab, which reached above 700 °C. The temperatures in the Traydec slab only reached about 400 °C due to its greater volume of concrete and therefore its added thermal capacity. The temperatures on the unexposed side of the slabs were also recorded and were compared to an insulation criterion limiting temperature rise on the unexposed side to less than 140 °C. This criterion met the design duration in all specimens except the Hibond slab. For this specimen, the expected fire resistance according to the manufacturer's design manual was 105 min which overestimated the true insulation time by a marginal 2 min. By the end of the 3-h exposure all specimens had exceeded 140 °C on their unexposed side.

The central deflections of all slabs are plotted in Fig. 3 (a). The deepest specimen, Traydec, had the least severe deflection reaching a maximum just above 125 mm. The reinforcement ratio had a pronounced effect on the deflections of the flat specimens. The most heavily reinforced flat slab HD12 reached a maximum deflection of about 155 mm, compared to about 200 mm and almost 270 mm for specimens 661 and D147 respectively. Despite having different magnitudes of deflection, all slabs demonstrated a very similar deflection pattern.

In the early stages of the fire, the deflection of the flat slabs was rapid until about 30 min, at which point the deflection rate declined. The initial slope change takes place in both composite slabs at a significantly earlier point in time corresponding to the time between 10 and 15 min. This may be related to the presence of the steel decking which would slip away from the concrete and provide radiation protection. Lim and Wade [23] also note that a pocket of air between the buckled steel decking and slab may have provided additional insulation thus reducing the temperatures in the slab in the early stages of the thermal exposure. This explanation is reasonable since in the early stages of a fire thermal expansion is dominant. However, upon closer inspection of the experimentally recorded temperatures such as those of specimen HD12 and the Hibond composite slab at a depth of 30 mm from the exposed surface as shown in Fig. 3 (b), this justification becomes less compelling. While it is true that the flat slab has higher temperatures, no significant difference in internal temperature increase rate as shown in

Fig. 3 (b) is observed between the flat and composite slabs, which means that the rate of temperature increase is not responsible for the different rate of deflection early in the fire.

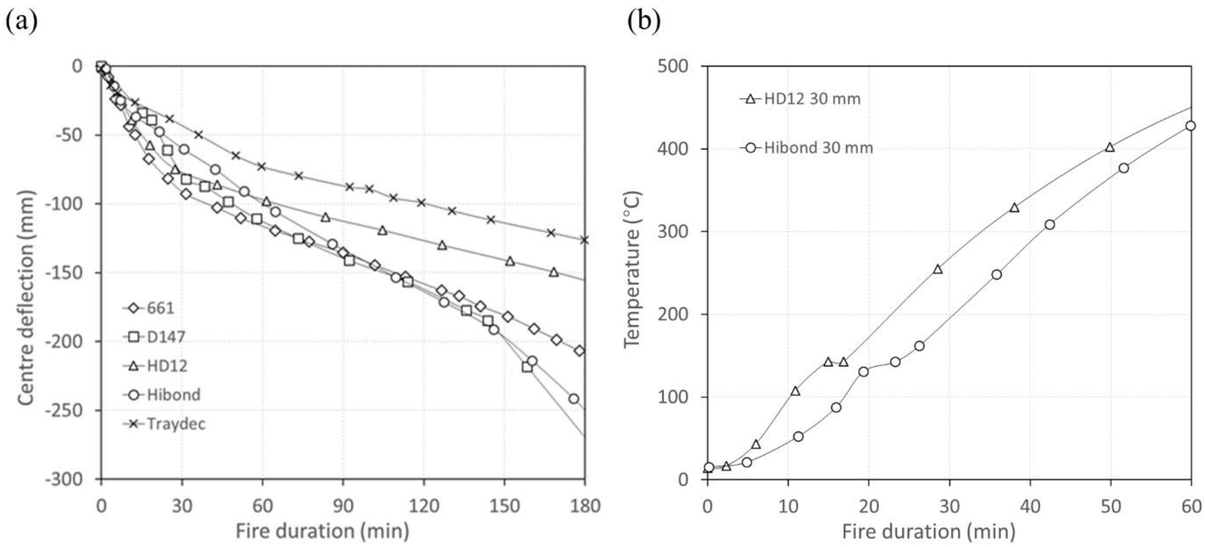

Fig. 3. Results from the BRANZ tests [23] (a) deflections for all specimens, and (b) recorded temperatures 30 mm away from the exposed surface

The cracking patterns for all tested slabs were similar with transverse cracks occurring across the short direction and over the corners. The first tests had diagonal cracks appearing from the corners and propagating towards the middle of the slab. This process was more rapid in the slabs with the clamped corners, with the additional manifestation of 45° cracks across the cross section that met with the diagonal surface cracks. In all specimens tested, cracks in the middle of the slab appeared and propagated across the short direction. The short direction cracks were transverse to the ribs of the ribbed slabs. These cracks appeared at regular intervals comprising multiples of the reinforcement spacing and penetrated through the depth when reaching the supports as shown in Fig. 4 (a) for specimen D147. Cracks parallel to the longitudinal slab edges also appeared in 661, D147, and the Hibond slab. In addition to these cracks, a large longitudinal crack appeared in the middle of D147 and the Hibond slab and penetrated through the depth of the specimen. No cracking was observed on the underside of specimens 661 and HD12 after the experiment, and no spalling was observed in any of the flat slab tests. Many of the cracks that had appeared on the top surface of D147, however, were clearly visible on the underside as well which can be seen in Fig. 4 (b).

After the test, the steel deck was detached from the concrete and significant spalling in the concrete was observed and kept in place by the steel deck. This was not observed in the Traydec slab for which the steel deck had debonded from the concrete but stayed in place due to the steel anchors. Another interesting crack observed in the Hibond specimen was a through-depth shear-like crack separating the rib and flat of the slab. This kind of crack, as will be seen, was observed in other experiments such as the Tongji and the Michigan State Composite floor tests [20, 21].

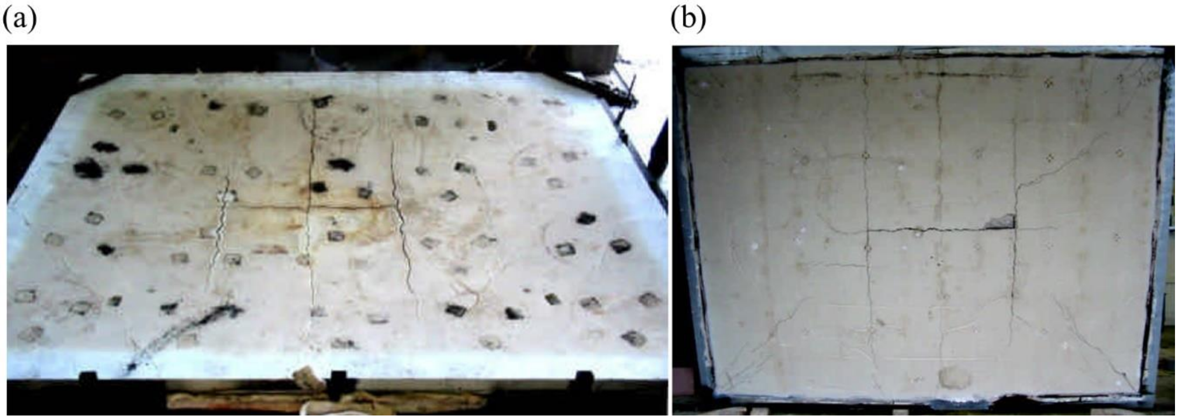

Fig. 4. Cracking in D147 appearing in the (a) top surface, and (b) bottom surface [23]

The BRANZ tests comprise a fundamental piece of experimental work regarding the behaviour of reinforced concrete and steel-concrete composite slabs in fire. Three-hour exposure to standard fire is likely beyond the realm of temperatures most structural elements are expected to be subjected to but the tests provided a valuable dataset for future work. The free boundary conditions and long thermal exposure allowed for very large deflections up to the order of *L*/13 to develop. In all specimens, the most fundamental cracks appeared around the centre of the slab and propagated across the short direction indicating that the tensile stresses and concrete damage were highest across that location. While diagonal cracking also formed, these cracks were not very significant. From the results of this study, there did not seem to be any significant difference between composite behaviours and flat slabs.

2.2. University of Manchester Small Scale Tests

Bailey and Toh [25] performed a series of 44 small scale tests on flat slabs at both ambient and elevated temperatures at the University of Manchester between 2004 and 2006, and published in 2007, to assess and refine the yield-line approach for modelling slabs in fire. The samples tested had one of two footprints: 1.2 m × 1.2 m or 1.8 m × 1.2 m, both of which had a thickness of 20 mm with a 5 mm concrete cover. There were 24 specimens reinforced with stainless steel bars, while the other 20 specimens utilised mild steel wires. The wire mesh used for reinforcement of the specimens had wires as thin as 0.68 mm in diameter and as thick as 3 mm, spaced between 6.35 mm and 50.8 mm apart. As per the actual specimen and reinforcement dimensions, this resulted in reinforcement ratios between 0.21% and 0.82% but with different steel grades and ductility. The reinforcement type and ratio were intended to be similar to those used in steel-concrete composite floor systems.

All specimens were supported on rollers with gently clamped corners allowing rotation and lateral translation. The samples were separated into two groups each consisting of 22 specimens. One group was tested at ambient, and the other was tested at elevated temperatures. A test load, different for each slab and highly dependent on logistical constraints of the experimental set-up, was first applied and maintained and then the furnace was turned on. The temperature in the electrical furnace with a heating rate of 300 °C/h was allowed to climb up to 1000 °C in just under 3.5 hours and then maintained until the failure of the specimens. The very thin thickness of the specimens, less than even the typical cover of real reinforced concrete members, makes the temperature profile achieved in the specimens unrepresentative of real fire scenarios.

The tested specimens failed at different levels of deflection which correlated with their reinforcement levels. Bailey and Toh [25] updated the yield line method to predict the level of deflection at which failure would occur and showed that it compares favourably with the ultimate deflection of some of the experimental observations as shown in Fig. 5 (a). Failure occurred due to rebar rupture across the short direction as shown in in Fig. 2 (b), or because of concrete crushing at the corners of the specimens. Rebar rupture across the short direction typically occurred when the slabs were lightly reinforced, while the compressive failure took place in more heavily reinforced specimens or specimens reinforced with ductile reinforcement such as stainless steel. The University of Manchester [25] tests presented here provided a basis for validating and updating the yield-line design method. The failure mode and cracking observed indicate that simply supported slabs are likely to fail by reinforcement rupture across the short span or by concrete crushing at the corners.

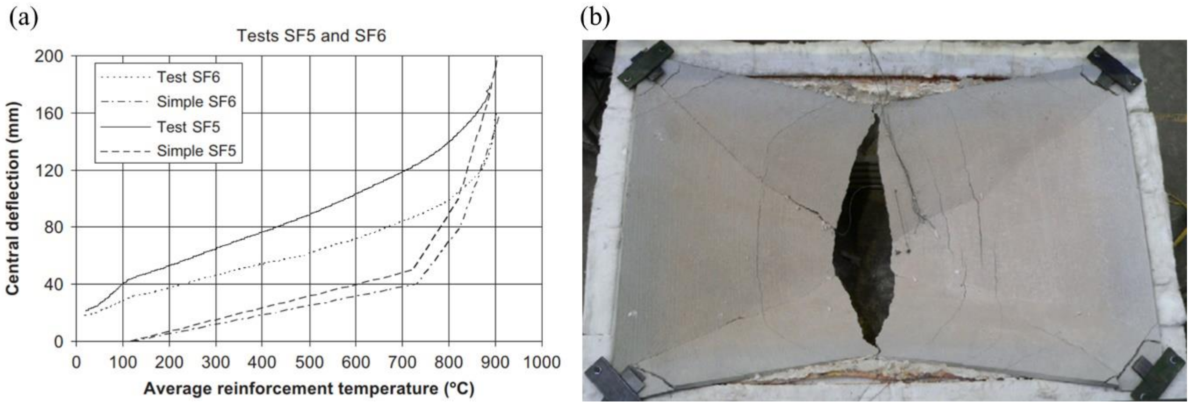

Fig. 5. Results from the University of Manchester small scale tests [25] (a) comparison between analytical predictions by yield line and experimental values, and (b) typical failure by reinforcement rupture

2.3. The University of Sheffield Small Scale tests

Researchers at the University of Sheffield performed two sets of elevated temperature tests on thin, lightly reinforced small-scale flat slabs and published their results in 2006 and 2008 [18, 19]. In addition, a set of tests was also performed on similar specimens at ambient [26]. This section will focus on the elevated temperature tests. The specimens in the two testing programmes were very similar. The tests by Foster [18] considered both square slabs with dimensions of 600 mm × 600 mm, and rectangular panels with an aspect ratio of 1.55 corresponding to a footprint of 920 mm × 620 mm. Following the Foster tests, Abu [19] tested 13 specimens with a length and width of 900 mm and 600 mm respectively. While Foster's specimens had nominal thicknesses within the range of 15 mm and 24 mm, Abu's specimens all had a nominal thickness of 15 mm [18, 19]. Foster reported the results of 25 tests, 14 of which utilised 'smooth' reinforcement wires while the rest used deformed wires [18].

Likewise, Abu reported the results of 13 tests, 5 of which used smooth wires and 8 were reinforced with deformed reinforcement wires [19]. The reinforcement ratios tested by Foster ranged from as small as 0.05% to as large as 0.25%, while Abu focused on more heavily reinforced specimens with reinforcement ratios between 0.1% to 0.5% [18, 19]. Foster's square slabs were loaded over 4 points, while her rectangular specimens were tested using a 12-point loading apparatus which Abu also utilised in his investigation. Both researchers used the same custom electrical furnace set-up, with fans added to prevent the overheating of the electrical heating coils. Heating was applied until failure or up to about 225 minutes in the Foster tests, or until central deflection rate reached zero in the Abu tests [18, 19]. In both test sets ambient load was applied before thermally loading the specimens, but in the Abu tests ambient load was maintained for 60 minutes before starting the furnace. While the furnace was capable of reaching up to 700 °C, the Abu specimens reached a maximum bottom temperature of about 600 °C, and the maximum bottom temperatures reported by Foster which approached the maximum furnace temperature of 700 °C [18, 19]. Similar to the Manchester tests, the scale of the specimens meant that their thermal profile may not be correspond to the expected thermal conditions within real structures.

Up to 300 °C, Foster noticed that the displacement of the specimens was similar independent of the reinforcement type, its amount, or the magnitude of the applied load. At higher temperatures, however, lower reinforcement ratio was surprisingly correlated with a higher central displacement. Thicker slabs tended to have lower displacement, and square specimens performed better than rectangular slabs at higher temperatures. Transverse cracks dominated the damage pattern of the specimens, with yield line cracks also appearing in some slabs particularly during the cooling phase. Reinforcement rupture and debonding were observed in some of the tests, but none of the specimens failed due to crushing of the concrete in the corners. This was not the case in the Abu tests where the corners crushed in 3 of the 13 specimens tested. This crushing was judged to have been the cause of the failure, but consideration of the failure shape prompts the authors of this review to suggest that the compressive failure of the Abu specimens was shear failure. The loaded area had penetrated into the slab along with a sudden increase in the central deflection rate, which is indicative of shear failure. This failure also occurred during the ambient loading stage for specimens subject to the highest loading ratios, which further supports the shear failure hypothesis.

The tests performed by Foster and Abu at the University of Sheffield provide an important source of data on the failure of slabs in fire. Many of the tested specimens reached failure caused by rupture of the reinforcement either across a central transverse crack, or within the yield line cracks. Moreover, many specimens did not manifest the yield line crack pattern at all, while others developed it only during the cooling phase. However, the scale of the specimens with a thickness of only 15 mm to 24 mm make these specimens not representative of real floor slabs, similar to the Manchester University tests presented by Bailey and Toh [25]. Size effects are important for slabs and in fire, and as such care must be taken when using the data from these tests.

2.4. Imperial College Tests

Tests conducted at Imperial College London and published in 2009 [27, 28] aimed to understand the relationship between bond strength, ductility, and ultimate capacity of lightly reinforced floor slabs in fire. 20 two-way slab specimens were built and tested at ambient conditions with different dimensions, rebar type, concrete strength, reinforcement ratio and arrangement. Eighteen of the twenty slabs were tested with simply supported boundary conditions, while two were tested with restrained edges. Reinforcement bar description and the corresponding material properties are provided in Table 2, where f_{sy} is the yield strength or 0.2% proof stress, f_{su} is the ultimate strength, and ε_{su} is the ultimate strain. The four specimens that used a profiled decking were stripped of it before testing to simulate loss of steel deck in fire conditions due to buckling and debonding.

Table 2. Rebar type and properties based on average of at least 3 samples [27]

Designation	Description	steel type	f_{sy} (MPa)	f_{su} (MPa)	ε_{su}
D8	Deformed bars with 8 mm diameter	cold-worked	551	624	0.05
D6	Deformed bars with 6 mm diameter	cold-worked	553	602	0.04
M6	A142 welded mesh of 6 mm deformed bars	cold-worked	550	589	0.025
P6	Plain bars with 8 mm diameter	hot-rolled	249	330	0.21

During testing, the specimens were placed over a stiffened steel frame supported on four concrete blocks fixed to the lab floor allowing rotation and translation at the slab edges. For the two fixed edge tests, additional steel framing was bolted to the existing framing providing lateral and rotational restraint around the edges of the specimens. The load was applied at 12 points on the face of the slab using a custom-built apparatus consisting of steel sections, plates, and ball joints ensuring equal distribution of force. The loading apparatus approximated distributed load which was applied until failure of the tested specimens.

All tests were performed to failure at ambient conditions. It was believed that the failure mechanism uncovered would be similar to what would be observed in fire and that thermal exposure may simply accelerate the process. In the case of restrained edges, thermal expansion and its induced forces would likely dominate the behaviour and reduce the reliability of the ambient test in representing thermomechanical behaviour. For this reason, the restrained specimens will not be discussed further in this section. The load-deflection history of the tested specimens was variably influenced by the different parameters that were changed, particularly the rebar type and its strain hardening. As shown in Fig. 6, the specimen with the plain rebars R-F60-P6-A reached significantly larger deflections and lower load before reaching failure. On the other hand, specimens with the deformed rebars obtained higher ultimate capacity but failed at almost half the deflection capacity. Cashell et al. [27] delegated this effect mostly to stress concentration in the rebars causing early failure. It must be noted, however, that the plain rebars used hot-rolled steel with an ultimate strain of 0.21, which is between 4 to 8 times the ultimate strain of the other deformed bars as shown in Table 2. Furthermore, the ultimate strength of the plain bars was also about half that of the deformed bars explaining some of the difference in ultimate capacity.

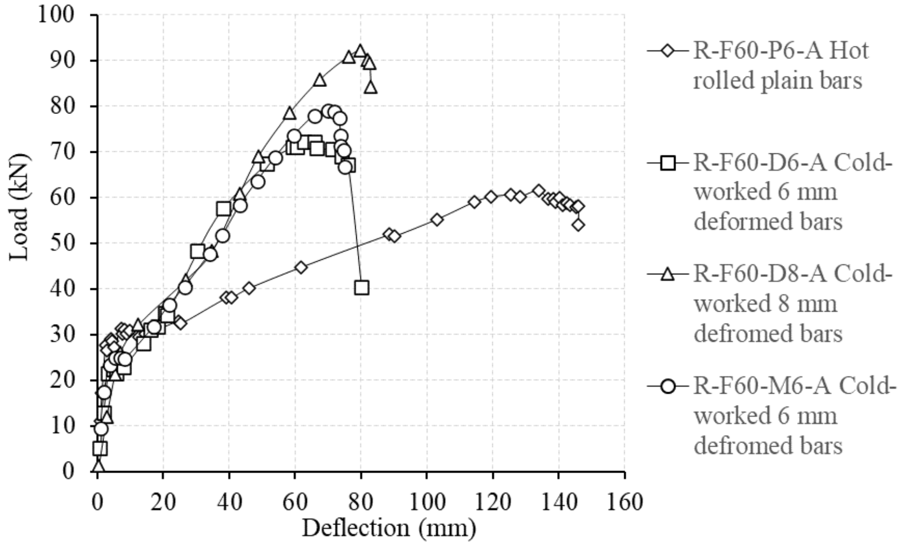

Fig. 6. Comparing the load-rotation relationship for specimens with different reinforcement types [27]

Failure in the tested specimens occurred in one of three mechanisms: (1) Rupture of the rebars, (2) Crushing of concrete, or (3) Punching shear. Out of 18 tested specimens, 13 failed in tensile rupture of the reinforcement, three failed in compression, and two suffered from punching shear. The tensile failure of the reinforcement often occurred at through-depth cracks in the short direction and resulted in a sharp drop in the load-carrying capacity. Failure by crushing of the concrete in the compressive region occurred in the specimens that were heavily reinforced, and in which the D8 rebars demonstrated more strain-hardening than the other reinforcement types used [27]. The two specimens that were reinforced with plain rebars failed in punching. The absence of dowel action and confinement introduced by more strongly concrete-bonded reinforcement bars may have reduced the shear capacity of the specimen. This indicates that the plane rebars may have been capable of carrying tensile membrane action effectively, but the lowered shear resistance caused punching shear to govern the failure.

The tests presented in Cashell et al. [28, 29] were performed at ambient temperatures to explore the large-displacement behaviour and failure mechanisms. Significant attention was paid to the contribution of bond strength to failure, and important insights were drawn and used for validation of an analytical method discussed in Section 5.1.3. The effects of aspect ratio, reinforcement ratio, section depth, and reinforcement type were also amongst the investigated parameters. Extension of these results to the thermo-mechanical case was done numerically in follow-up work [28, 30, 31].

2.5. SEU Profiled Slab tests

Fan et al. [32] tested two concrete-steel composite profiled slabs subjected to 90 min of heating according to the ISO 834 temperature-time curve at the Southeast University (SEU), China and published the results in 2015. The slab 'sheets' had a footprint of 3 m × 1.86 m and were 130 mm deep. The concrete used in the experiment was particularly weak with a compressive strength of 11.9 MPa. The steel decking was 1 mm thick and had a yield strength of 235 MPa with 51 mm deep ribs 253 mm apart. A reinforcement mesh with 150 mm × 150 mm and 8 mm diameter bars was used as top reinforcement 25 mm below the surface of the slab. The reinforcement had a yield strength of 310 MPa. It is immediately clear that the concrete strength was too low to be characteristic of typical construction. This may cause different failure mechanisms to dominate (e.g. early concrete failure) and may not provide enough perimeter support to allow the slab to experience TMA. Regardless, these tests are still a useful datapoint as they were performed using ribbed slabs on steel decking and under elevated temperatures.

To produce fully restrained boundary conditions, a reinforced concrete rectangular beam was used around the perimeter of the slab as shown in Fig. 7. Mechanical load was applied over five on top of the slab. The slab specimen was placed over the furnace as shown in the figure, loaded mechanically at ambient, and then heating was applied as per the ISO 834 temperature-time curve. Temperatures and deflections were recorded throughout the experiment.

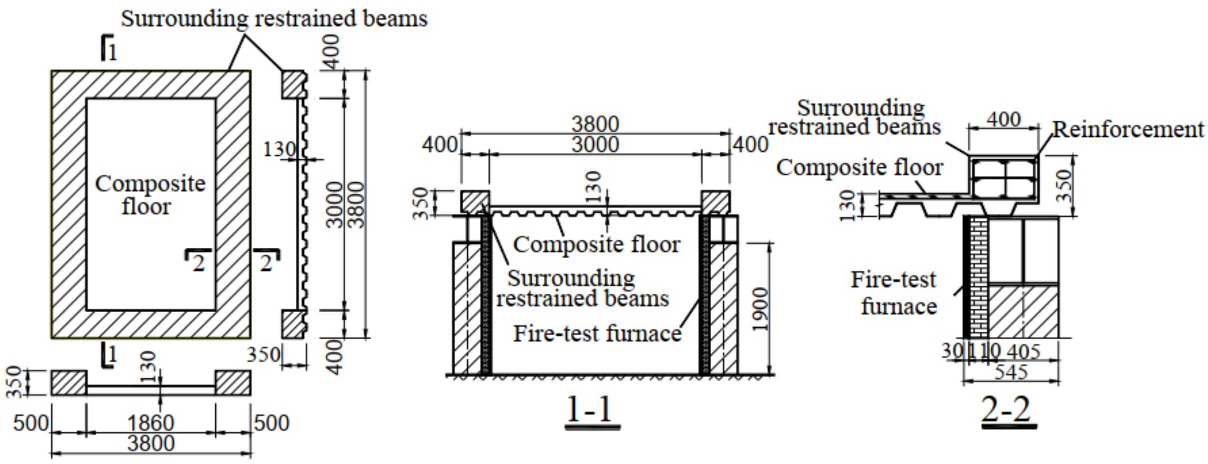

Fig. 7. Edge restraint for the tested specimens [32]

The furnace used in the experiment struggled to achieve the ISO 834 temperatures and there was a maximum difference of about 250 °C between the two. Despite this, the furnace temperatures were on average within 100 °C of the ISO 834 curve especially in the later stages of the test. Slab bottom temperatures lagged behind the furnace temperatures until about 70 min into the test, when they reached a maximum temperature of nearly 800 °C. The temperature of the unexposed surface reached about 90 °C. The temperature of the reinforcement bars remained just below 250 °C throughout the test.
The deflection was 19.5 mm ($L/95$) even before the thermal loading. Maximum deflections achieved during heating were about 110 mm and 90 mm, which is less than the total slab thickness but about $L/17$ and $L/21$ where L is the length of the short edge of the slab. The thermo-mechanical deflection

was a continuous line without any slope-change points, as cross-section cracking had already occurred during the mechanical loading as shown in Fig. 8 (a) and (b).

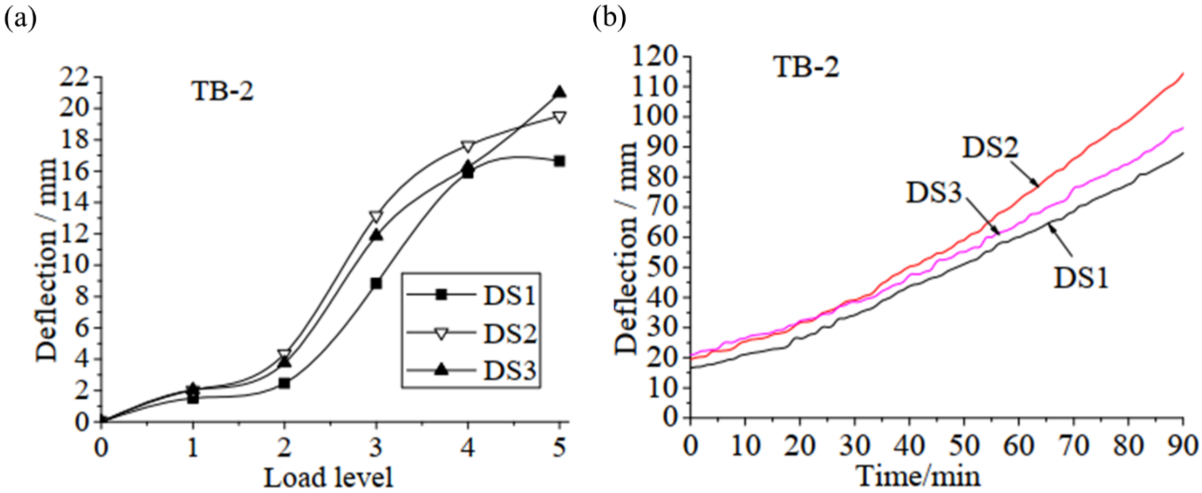

Fig. 8. Load-deflection of specimen 2 (a) mechanical loading, (b) thermal loading [32]

The first cracks were corner cracks and occurred during the mechanical loading stage. The cracks that developed during the heating phase were concentrated on the edges and corners of the slab. Cracks were also observed on the bottom of the slab and under the loading points. Unfortunately, the very low concrete strength and unclear photographs presented of the experimental observations make it difficult to interpret the crack patterns. However, even with concrete with about 30% - 50% the typical concrete strengths used in other experiments the specimens were able to achieve deflections as high as $L/17$ without collapse.

3. Tests on Composite Floor Assemblies

Composite floor assemblies denote a step-up from tests on simplified panels by including perimeter beams, and sometimes intermediate beams, in addition to the slab panel. While these tests may not fully represent continuity across the floor plate, they better capture the boundary conditions of composite floor systems by incorporating the edge beams. The inclusion of intermediate beams in some of the experiments also allow to test the hypothesis that these beams do not contribute significantly to the overall capacity of the floor system.

3.1. BRE Large Slab Test

Bailey et al. [33] performed a large scale ambient test to simulate tensile membrane action in composite slabs in fire at BRE Garston and published their findings in 2000. The floor slab cast had a footprint of 9.5 m × 6.5 m and was 150 mm thick with 60 mm deep ribs spaced 200 mm apart. The concrete was cast on ribbed shuttering without embossments and not on standard steel decking profiles. In addition, the steel profile used was greased and coated with cellophane to prevent bonding with the concrete. This was done to avoid damaging the specimen when the steel profile was ripped off the slab to simulate the assumed debonding and loss of steel decking due to elevated temperatures. An anti-cracking mesh was used to reinforce the specimen and was placed 15 mm atop the ribs. The wires were 6 mm in diameter and spaced at 200 mm in both directions. The average yield and ultimate stresses were 584 MPa and 641 MPa respectively with an average ultimate elongation of 12.2%. Grade C35 lightweight concrete was used, but no measured strengths were reported.

The slab was supported on all four edges over a steel frame with an overhang in both directions. In addition, a steel column with a roller was placed within the span of the edge beams to provide additional vertical restraint without additional rotational restraint. The edges of the slab were connected to a steel frame using Hilti HVB95 shear connectors spaced at 100 mm on the short edges (parallel to the ribs) and in pairs spaced at 200 mm on the long edge (perpendicular to the ribs). Each of the shear connectors had a capacity of 35 kN and were arranged to have an equivalent capacity to the shear connector arrangement used in the Cardington experiments. The load was applied over 16 points spread over the area of the slab.

The test was performed in three stages. In the first stage, the steel profile was removed which meant the slab had to support its self-weight of 2.3 kN/m^2 without the help of the steel deck. This self-weight resulted in the development of the yield-line cracks and a central deflection of 59 mm (*L/110*) [33]. In the second stage, the loading apparatus was installed and fitted to the slab to apply an equivalent uniform distributed load (UDL) which resulted in deflections reaching about 113 mm including about 4 mm of creep. In the last stage, an equivalent UDL of 3.65 kN/m^2 was applied followed by 1 kN increments at the load-points until the failure of the slab which occurred at an equivalent uniform load of 4.81 kN/m^2. The deflection-time curve for this last loading stage is shown in Fig. 9 (a), and shows that at failure the slab had a deflection of 700 mm. That is equivalent to *L*/9.3 where *L* is the length of the short direction.

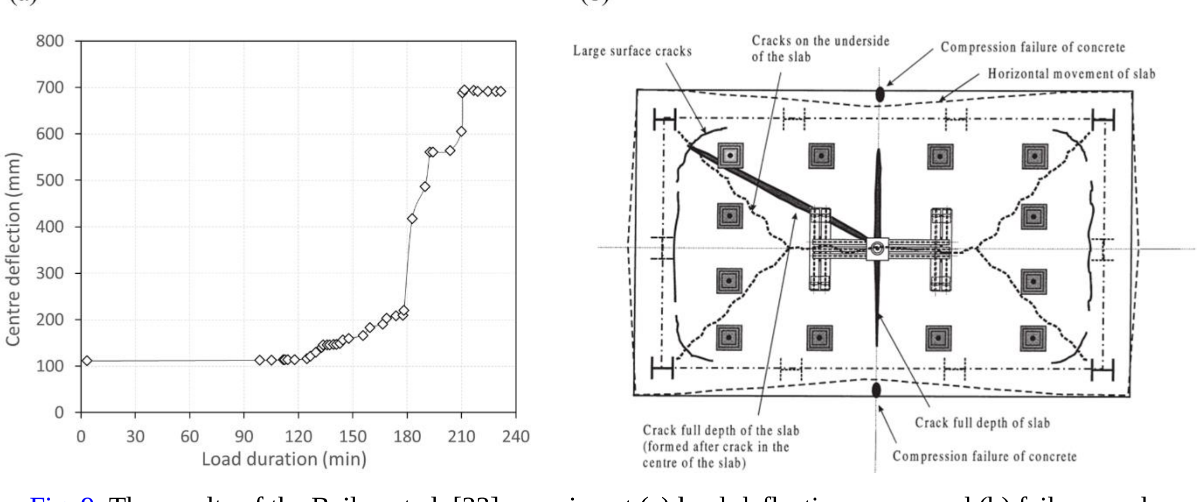

Fig. 9. The results of the Bailey et al. [33] experiment (a) load-deflection curve, and (b) failure mode

The slab failed when a central through-depth crack developed across the short span. The reinforcement mesh fractured within this crack, and the slab was divided into two sections allowing for another diagonal crack to form and cause ultimate failure of the slab as shown in Fig. 9 (b). Concrete crushing occurred in the middle span of the long direction at both ends from the central crack, and cracks formed at the corners and parallel to the short span as shown in the figure. Lateral inward deflection of the central point of the long span occurred at both ends as the tensile membrane action developed. The opposite occurred along the short span, however, with the edges pushing out. Bailey et al. [33] delegated this phenomenon to buckling of the short-direction beams which were under compression as they supported the large deflections of the slab.

This experiment was one of the earliest explorations of the failure of slabs in fire in tensile membrane action. It later served as an important validation case for the development of the Bailey design method for slabs in fire. The failure occurred as a result of tensile fracture of long-span rebars with a large through-depth crack forming across the short span. As Bailey et al. [33] note, however, one must be careful when extending the results of this experiment to the fire-dominated scenario. While large deflections may indeed be present, it is likely that the extent of these deflections, the stress state within the slab, and the material properties would be very different. The interaction between the supporting structure, slab, and shear connectors were insightful. While the long span pulled in due to large deflections, the short direction beams were pushed out.

3.2. Michigan State University Composite Floor Tests

Wellman et al. [21] tested three floor assemblies consisting of two girders supporting three beams on top of which a composite slab was cast on trapezoidal steel decking in fire. The tests were performed at Michigan State University and were published in 2011. To fit within the confines of the furnace, the assembly was scaled down to smaller sections that were meant to be representative of the strength ratios of real structures. Overall, the structural framing arrangement had a footprint of 3.96 m × 2.13 m and used W10×15 sections for the beams and W12×16 for the girders. Due to the constraints of the experimental set-up dictated by the furnace, both girders and the central beam were aligned within the furnace which had a heated area of 2.54 m × 3.12 m. A 101.6 mm lightweight concrete slab was cast on top of a 38.1 mm deep steel decking and reinforced with 3.4 mm diameter 152 mm × 152 mm spaced welded wire fabric mesh. The slab extended beyond the framing and had a total footprint of 3.96 m × 4.57 m. The slab was partially composite with a composite ratio of 32.5% with the beams, and 25.4% with the girders. Composite action was designed using headed shear studs with a diameter of 15.9 mm and a length of 76.2 mm. Two of the specimens used shear tab connections, and one used a double angle connection. Fire protection was applied to all members except the interior beams, which were only fire-protected in the control sample FA-1.

The ASTM E119 temperature-time curve was applied and maintained until the 'failure' of the specimens. The mechanical load was applied at five points: the centre of the slab atop the secondary beam, and at two points 864 mm apart about the centre of each of the two girders. The applied load corresponded to 46% of the moment capacity of the secondary beams. Once the load at the interior secondary beam exceeded its capacity, the vertical load was transferred to the girders to maintain the same bending moment within the girders as before the relocation of the load. The test was terminated, and cooling started when: a. the capacity of the girders was reached, b. the concrete at the loading point had been crushed, or c. the actuators ran out of stroke and no more load could be applied. The deflection and deflections rate limits used were those recommended by the BS-476: maximum deflection of $L/20$, or $L/30$ with a deflection rate of $L^2/9000$. Uncontrolled cooling corresponded, as per Wellman et al. [21], to unrealistic conditions and was applied to specimen FA-1. This was because the laboratory ventilation was increased by opening the shutters and vents which resulted in rapid cooling that a real structure would not be subject to. Controlled cooling at 12.2 °C/min was applied to the remaining specimens FA-2 and FA-3.

The temperature in the reinforcement mesh peaked well into the cooling phase. This was also the case for the shear studs. The maximum temperature reached in the shear studs was almost 600 °C at the midpoint of the secondary beam, while the wire mesh achieved a maximum temperature of about 300 °C. The temperature at the top surface of the concrete stayed below 100 °C for specimens FA-1 and FA-3 but reached about 200 °C in FA-2. Specimens FA-2 and FA-3 reached a maximum central deformation of about 250 mm, while specimen FA-1 had early explosive crushing of the concrete under the load point preventing the continuation of the central loading after 80 mm of deflection. Deflections of FA-2 and FA-3 indicate that they likely went into tensile membrane action. The authors noted, however, that the slab was unable to arrest the runaway failure of neither the beams nor the girders and so recommend not removing the fire protection of secondary members. It is difficult, however, to judge whether the slab could efficiently carry the applied loads in membrane action because of the load application method in which load was directly applied over the secondary beams. This procedure, for example, resulted in stress localisation that caused crushing of the concrete atop the midspan of the secondary beams.

The lateral displacement of the girder coupled with the rotation of the lower flange into the connected secondary beam observed in the experiment shows that the effect of thermal expansion may cause significant distortion of the floor framing. It is also noteworthy that all of the connections in the three specimens remained intact and did not fail. This shows that a protected connection designed considering elevated temperatures may indeed behave robustly in a fire. Diagonal cracking through the flat part of the composite slab, as shown in Fig. 10 (a), was observed in all tested specimens. Cracks of this type, as explained by Rezaeian et al. [34], whether parallel to the corrugations or in a diagonal direction to them, are a result of in-plane shear forces. Debonding was not indicated to have occurred [21], but inspection of the figure shows that it had taken place at the location of the aforementioned through-depth shear-like cracks. Closer inspection of Fig. 10 (b), however, shows that the decking was flush with concrete across the span of the slab where distortion of the cross-section did not occur.

Sample FA-3 experienced a large shear crack atop one of its girders during heating, and that resulted in larger deformations within that specimen. Yet again, the highly concentrated load in that location may have contributed to this occurrence and it is difficult to say with certainty whether such a localised failure was due to the load application, or due to thermally induced effects.

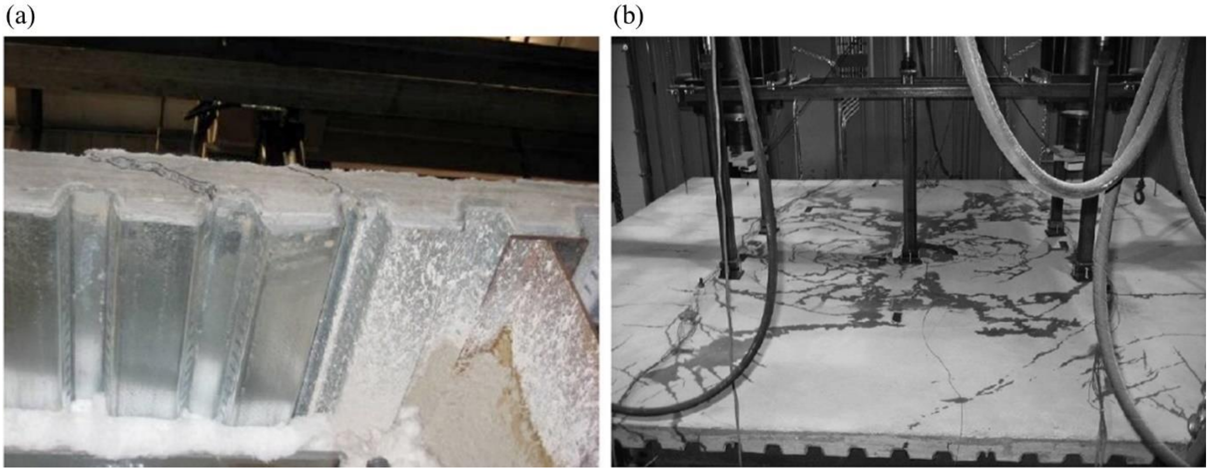

Fig. 10. Results from the Michigan State experiment [21] (a) Diagonal cracking in the flat part of the slab, and (b) surface cracking of the slab after initiation of heating

3.3. FRACOF & COSSFIRE

FRACOF and COSSFIRE were large scale composite-floor experiments documented in a series of technical reports by Vassart and Zhao [16, 35] and Zhao et al. [17] published in 2011. The two assemblies tested in FRACOF and COSSFIRE had footprints of 6.66 m × 8.735 m and 6.66 m × 9.0 m respectively as shown in Fig. 11. Both assemblies had a normal weight concrete slab cast on 58 mm deep 0.75 mm thick trapezoidal steel decking, and both used the same anti-cracking mesh with 7 mm diameter wires in a 150 mm × 150 mm grid. The continuous portion of the slab was deeper in the FRACOF experiment, however, with a total slab depth of 155 mm and concrete cover of 50 mm from the top face of the slab. COSSFIRE on the other hand used a 135 slab with a 35 mm concrete cover. Composite action with the steel framing was ensured using headed shear studs that were 19 mm in diameter and 125 mm in length placed 207 mm apart on the secondary beams. The shear studs were also used to ensure composite action with the primary beams with a spacing of 100 mm in FRACOF and 300 mm in COSSFIRE. The floor framing was designed per the ambient temperature requirements of the EN 1994-1-1 [1], the connections following the EN 1993-1-8 [36], while the thickness of the FRACOF floor slab was sized to provide sufficient insulation for 120 min fire resistance as per the EN 1994-1-2 [37].

In FRACOF, the primary beams, connections, and columns were protected. In COSSFIRE the connections were purposefully under-protected to allow for better assessment of their thermo-mechanical behaviour in fire. During the FRACOF experiment, the furnace walls were built in contact with the steel framing reducing the thermal exposure of the edge beams, while the entire frame was within the confines of the furnace during COSSFIRE producing a more severe thermal exposure. The mechanical load was distributed over the slab area using sandbags resulting in an applied load of 3.87

kN/m^2 for FRACOF and 3.93 kN/m^2 for COSSFIRE. Both experiments had the structural arrangements subjected to just over 120 min ISO 834 fire. At that point, the integrity of the floor was violated during the FRACOF test, and a secondary edge beam failed in COSSFIRE.

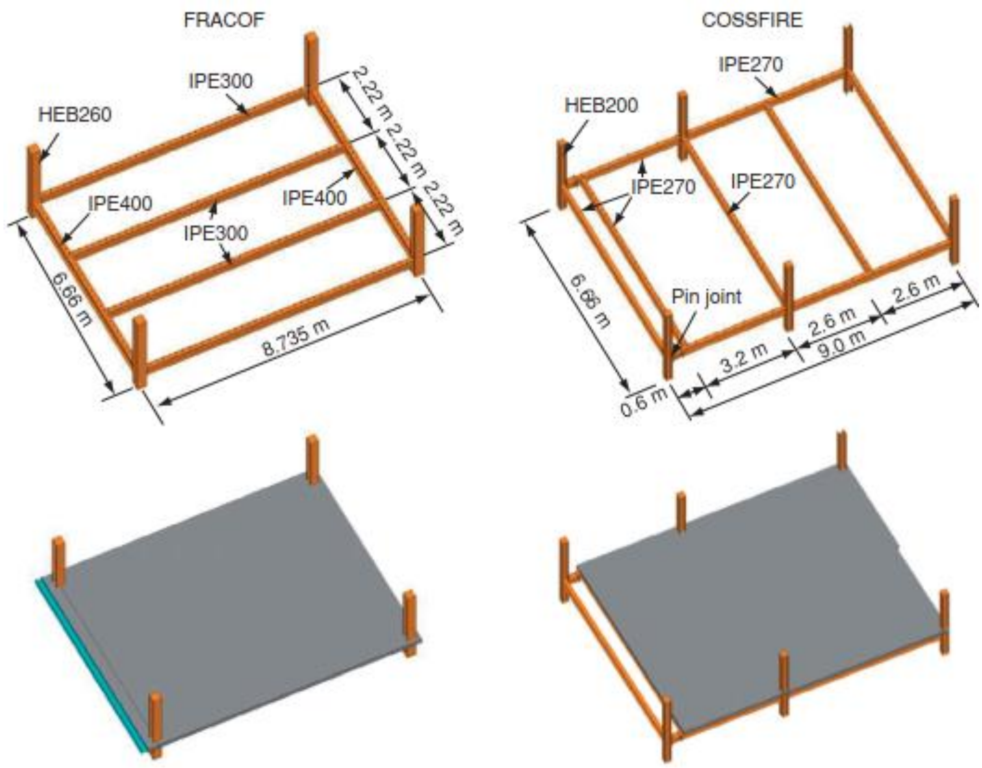

Fig. 11. Composite floors tested in FRACOF and COSSFIRE [38].

Furnace temperatures exceeded 1000 °C in both experiments, but the insulation criteria of temperature at the unexposed side of the slab remaining below 140 °C was only exceeded in the thinner slab of COSSFIRE. In that test, the unexposed face reached above 200 °C compared to just over 100 °C for FRACOF. This also corresponded to a higher reinforcing mesh temperature of about 500 °C in COSSFIRE compared to 300°C in FRACOF. Both these temperatures were reached during the cooling stage. Moreover, due to the aforementioned arrangement of the furnace walls in FRACOF, the edge beams remained at around 300 °C compared to an average edge beam temperature of 550 °C in COSSFIRE. The reduced thermal protection on the connections in COSSFIRE resulted in their temperatures reaching 800 °C compared to only 300 °C in FRACOF. Overall, despite the two structures being subjected to similar furnace temperatures, COSSFIRE had significantly higher temperatures compared to FRACOF. This was a result of the arrangement within the furnace, the thinner slab used in COSSFIRE, and the reduction of fire protection on the connections.

Due to the higher temperatures, it is expected that the COSSFIRE experiment would experience larger deflections, and indeed the central deflection was about 550 mm compared to 450 mm in FRACOF, which corresponds to a deflection to short span ratio of L/12.1 and L/14.8 respectively. It is evident that such a deflection far exceeds the L/30 failure criterion. With secondary internal beam temperatures reaching 1000 °C, it is expected that the contribution of tensile membrane action to the load resistance was significant. Studying the deflection-time history shown in Fig. 12, it is noticeable that up to the 30 min of the fire the deflection paths were similar, and both reached a maximum deflection to short span ratio of about *L*/27.

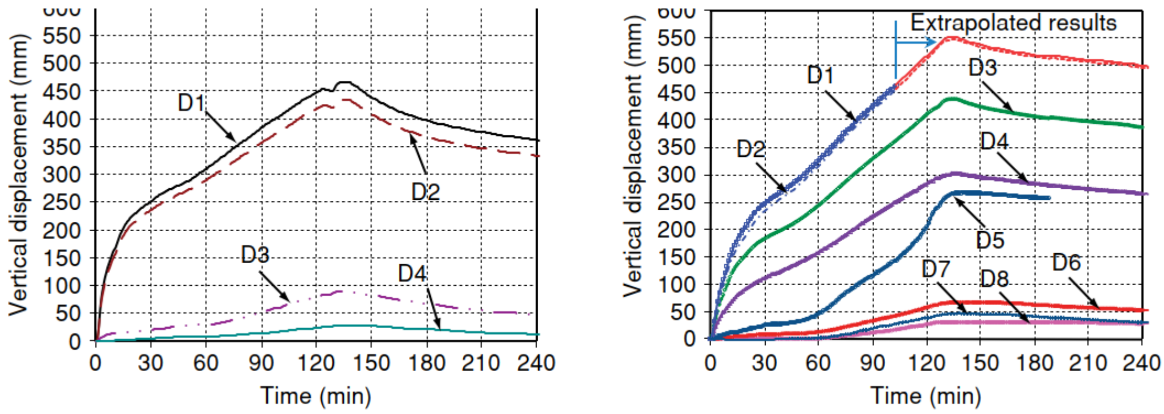

Fig. 12. Load-displacement of the central point in FRACOF and COSSFIRE. Reproduced from [38]

At this point, the temperature in the bottom flange of the unprotected beams was above 800 °C for both experiments indicating severe degradation in capacity. This indicates that even early in the fire, due to the very high temperatures in the secondary internal beams, material degradation may have contributed to the deflection. It is expected, however, that the large thermal gradients generated by the difference in temperature between the unprotected steel sections and the concrete slab would have had a more pronounced effect and likely dominated the behaviour.

During the testing, cracks appeared at the corners diagonal to where the columns were in both experiments as shown for FRACOF in Fig. 13. These cracks did not seem to cause any negative effects to either load carrying capacity or insulation of the slabs. A central crack did develop in the FRACOF experiment, but it only occurred due to poor overlapping of the reinforcement and did not appear to have an impact on either the load-carrying capacity, deflection history, or insulation failure criteria of the slab. Debonding of the steel decking was observed over a large part of the slab.

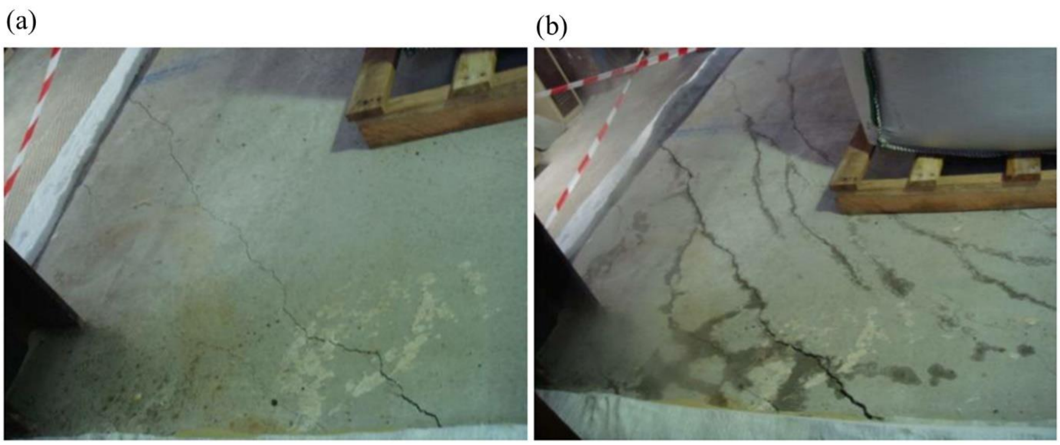

Fig. 13. Cracks at the corners of the FRACOF slab (a) beginning of the fire, and (b) end of the fire [16]

In COSSFIRE, buckling of the internal secondary beam where it connected to the column occurred. The other unprotected internal beam that connected to the girder did not experience this local distortion. Failure in this experiment occurred due to one of the edge beams reaching runaway failure, due to faulty fire protection resulting in it reaching temperatures over 600 °C. Concrete on top of this beam crushed, but its collapse did not affect the overall integrity of the structural assembly.

Other than the aforementioned local failures, there was no report of debonding of the steel decking, no signs of shear slip, nor was any failure noted in the connections even in the COSSFIRE experiment where they had reached temperatures over 800 °C. In particular, no large cracks developed over the edge beams due to hogging moments, which, as noted by Bisby et al. [39], may have been caused by low edge torsional restraint. Slab continuity was not simulated in the experiment, and thus large hogging moments could not have developed, and cracking in the concrete over the supports did not occur. Instead, the aforementioned diagonal cracking around the columns occurred due to the restraint provided by the columns against both translation and rotation. The detailing of the column-slab connections included the addition of extra reinforcement, which may have limited the extent of the cracking there and prevented cracking from jeopardising the structural integrity of the slab at these locations.

The overall performance of the structural assemblies as displayed in both FRACOF and COSSFIRE was robust. Despite the localised failures that took place, system collapse did not occur and in both tests the slabs met the 120-minute load-bearing period they were designed for. The absence of clear photos of the crack pattern during and after the fire makes it rather difficult to make many comments about the mechanism of the development of tensile membrane action, although the exceptionally large displacements coupled with very high internal beam temperature would have caused its occurrence. Given that Vassart and Zhao [16] indicated the absence of any significant cracking beyond what was already mentioned, it may be safe to assume that yield line cracks were not visible. Furthermore, the absence of data about the lateral displacement of the columns makes it challenging to gauge the lateral tractions the slab exerted at the various stages of the fire before and after potential development of TMA.

3.4. NTU Scaled Composite Floor Tests

Nguyen and Tan [40, 41] and Nguyen et al. [42] tested a total of eight quarter-scale assemblies of flat slabs composite with steel framing supported on steel columns. The tests were performed at the Nanyang Technological University (NTU) and the results were published in 2015. All specimens had the same footprint: 2.25 m × 2.25 m slab with 0.45 m overhang which was used to simulate edge continuity of internal panels in real structures. The columns were designed to be particularly stiff relative to the rest of the assembly to prevent column failure or deformation from dominating the structural behaviour. In all specimens, the slab was designed with a target depth of 55 mm. As would be expected for flat slabs of this scale, the actual depth of the slabs varied between 55 mm and 59 mm. The experimenters did not use ribbed slabs on corrugated decking because they were unable to source a decking with appropriate dimensions. A 3 mm diameter 80 mm × 80 mm shrinkage reinforcement mesh was used without lapping over the entire area of the slab. This corresponds to a reinforcement ratio of only 0.16%, which is lower than ratio for the University of Manchester tests [25] but higher than the minimum specifications set out in the EN 1994-1-1 [1]. Headed shear studs that are 40 mm long and 13 mm in diameter were placed at 80 mm spacing to provide full composite action between the steel framing and the slab.

The eight specimens were presented in the literature over three groups each of which focused on varying one parameter while keeping the others unchanged. The first set of specimens (S1, S2-FR-IB, and S3-FR) is shown in Table 3 and presented in [42] focused on assessing the effect of rotational edge restraint, and the impact of removing interior secondary beams or keeping them unprotected. Nguyen and Tan [40] later presented the results of another set of tested specimens (P215-M1099, P368-M1099, and P486-M1099) where the size of the secondary edge beam was changed while keeping the rest of the assembly constant. The last set of results (specimens P215-M1356 and P215-M2110) changed the size of the primary edge beam and compared them to the control specimen P215-M1099 [41].

Table 3. Specimen information for the NTU tests [42]

Specimen	**Primary edge beams**	**Secondary edge beams**	**Secondary internal beams**	**Concrete mean strength (MPa)**
S1[1]			_	36.3
S2-FR-IB[1]		80 × 80 × 17.3	80 × 80 × 17.3	36.3
S3-FR[1]	W130 × 130 × 28.1		_	31.3
P215-M1099[2,3]				31.3
P368-M1099[2]		100 × 80 × 18.8		32.9
P486-M1099[2]		102 × 102 × 23	80 × 80 × 17.3	28.9
P215-M1356[3]	UB 178 × 102 × 19	80 × 80 × 17.3		32.9
P215-M2110[3]	UB 203 × 102 × 23	100 × 80 × 18.8		28.9

[1][42]; [2][40]; [3][41]

The reason all specimens were cast at a 1/4 scale was to fit them within the confines of the 3 m × 3 m × 0.75 m electrical furnace at NTY. The slab was on top of the furnace, while the protected columns and both protected edge beams and unprotected interior secondary beam were subjected to heating at a rate of 20 °C/min. Mechanical loading equivalent to 15.8 kN/m^2 was applied using a 12-point loading system that ensured the load was vertical during the tests. The temperatures at various points within the assembly were recorded, and so were the deflections, including the lateral deflection of the columns. The tests were aborted when either edge-beam full-depth cracks opened up to 10 mm or when the load level could no longer be maintained due to loss of stiffness [43]. This was the point of failure as defined to in this experimental study.

Beam-column and beam-beam connections were flexible end plate connections, and the column ends were connected to a supporting base that was pin-connected to the strong floor of the laboratory. The defining feature of this set of experiments, except for specimen S1, was the edge restraint conditions. Samples S2-FR-IB and S3-FR both had a rotational restraint system that prevented their upward rotation. Samples P215-M1099 through P215-M2110 all had, in addition to the rotational restraint system, an in-plane restraint system that only allowed finite translations of the slab edge in a straight line. This system consisted of five M24 bolts cast into the slab with half their length exposed and connected to the rotational restraint with a 20 mm gap between the tip of the bolts and the furnace wall. A specimen with the protruding bolts is shown in Fig. 14. This allowed for a good simulation of slab edge continuity as would be the case in real multi-bay structures.

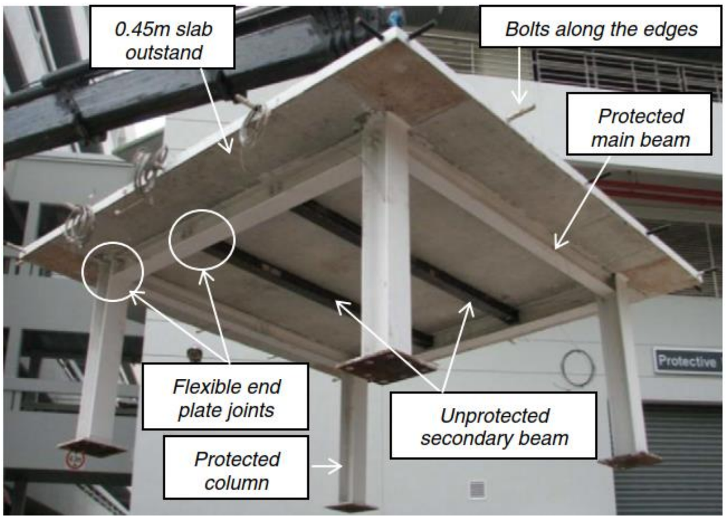

Fig. 14. Specimens used in the NTU tests [40]

The furnace in the experiments was electrical and its heating rate was limited by the maximum possible power input, which meant that it was incapable of heating the samples as per the ISO 834 temperature-time curve. It was, however, capable of achieving a heating rate of about 20 °C/ min. Most test specimens experienced maximum furnace temperatures between 800 °C and 1000 °C at around the 100 min mark. Specimens S3-FR and P215-M2110 were exceptions as the furnace air temperature had reached a maximum of around 800 °C and 820 °C within 59 min and 200 min respectively. S3-FR had reached the point of failure at 59 min and so the test did not continue. The slow heating of P215-M2110 was due to a damaged heating element. The temperatures for the protected edge beams reached over 800 °C and were hotter than the bottom surface of the slabs. It must be noted that since this experiment was performed on scaled specimens, the temperature distribution in the various components could not be as representative as full-scale experiments. For example, the deepest heated edge beams were only 203 mm deep.

The average deflection ratio at failure in all the tested specimens was *L*/16.9, with the highest ratio of *L*/12.7 achieved in S2-FR-IB, and the smallest about *L*/19.5 in S3-FR. Instead of referring to this ratio, however, the authors of the studies [40–42] refer to deflection as a multiple of the slab depth. This is a particularly useful measure as it helps assess the potential for tensile membrane action, which Nguyen and Tan [40, 41] and Nguyen et al. [42] note occur at the point when the central deflection just exceeds the slab depth. One of the strengths of the NTU studies is that they were able to break down the deflection-temperature history into distinct stages. The edge beams, for example, went through the following deflection stages defined in Nguyen et al. [42] and shown in Fig. 15 (a).

In phase 1, restrained thermal expansion results in increased deflection enhanced by the gradient between the slab and beam. In phase 2, the temperature of the slab begins to increase resulting in a lowered thermal gradient and a brief reduction of deflection, which is then overcome, and deflections increase. Finally, phase 3 occurs after the beams reach a temperature range between 650 °C and 700 °C and enter a runaway deflection phase.

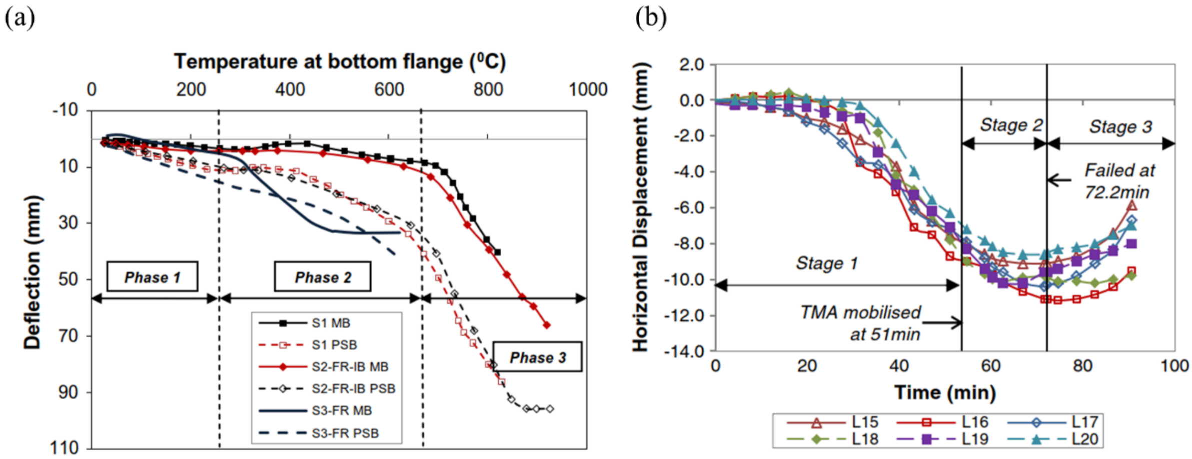

Fig. 15. Displacement results for some of the NTU tests [40, 42] (a) Mid-span deflection of edge beams against temperature, and (b) horizontal displacement-time curve for P215-M1099

These phases are also present in the other sets of specimens [40, 41] but are not as prominent. Perhaps what is more novel about the data analysis provided by Nguyen and Tan [41] and Tan and Nguyen [40] is the description of lateral translations of the slab edges. As aforementioned, the boundary conditions of this experiment allow for only straight-line translation of the edge as would be expected for internal panels in a fire. The observed lateral deflections shown in Fig. 15 (b) were also divided into three stages. The first stage is characterised by outward expansion of the slab edge governed by thermal expansion. The rate of this expansion is first limited due to heat build-up and then increases rapidly after the evaporation of slab moisture content. In the second stage, the beginning of tensile membrane action begins to curtail the outward expansion resulting in what Tan and Nguyen [40] refer to as a "near-constant" displacement rate. In Stage 3, inward deflection takes over completely and runaway failure occurs due to cracks above the edge beams. Analysing the same figures for the other specimens provided in [40, 41], however, it is rather difficult to differentiate between the end of Stage 1 and beginning of Stage 2 where tensile membrane action is supposed to have developed.

Column displacement offers a more holistic picture of the state of the slab as the tractions transferred into the columns cause them to move laterally [40]. This is clear by considering the horizontal displacement of the columns shown in Fig. 16 (a). In the beginning, the column is pushed out due to the expansive tractions developed in the slab, until the development of tensile membrane action at which point the tractions reverse and become tensile pulling the columns in. This pattern was consistent in all the specimens shown in the figure. The vertical displacements of the columns are shown in Fig. 16 (b) and indicate the same mechanism. As heating starts, the columns start expanding and thus deflect upwards. At the onset of the tensile membrane action, the columns are pulled downwards by tensile tractions in the slab.

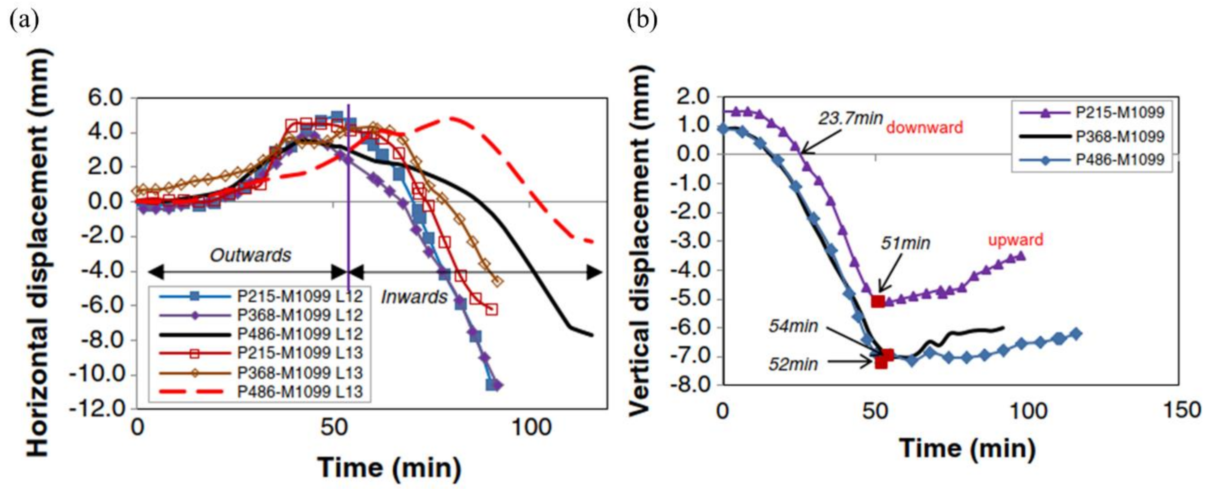

Fig. 16. Displacement results for the columns from Tan and Nguyen [40] (a) Column lateral displacements, and (b) Column vertical deflections

All specimens showed three fundamental cracking patterns: (1) Early in the heating of all tests, diagonal cracks at 45° angles formed at the column locations, (2) The compression ring began to form at the time when the deflection at the centre of the slab approached the depth of the slab with diagonal cracks connecting edge-cracks in the shape of a ring, and (3) Through-depth cracks formed over the edge beams and the reinforcement ruptured in those locations. In some specimens, cracks developed within the central region and over the secondary internal beams. These cracks were not very impactful and the reinforcement along them did not fail. No yield-line-like pattern occurred in any of the specimens tested as can be seen in Fig. 17. Other than this, no buckling of columns occurred, nor did local distortion of beams at their connections take place. The absence of local buckling in the framing may be due to the flexible connections used. There were no signs of loss of composite action or failure of shear studs, but the large cracks over the edge beams are stipulated by the experimenters to have acutely reduced compositeness and thus nullified the beneficial effects of stiff edge beams rather quickly in the fire.

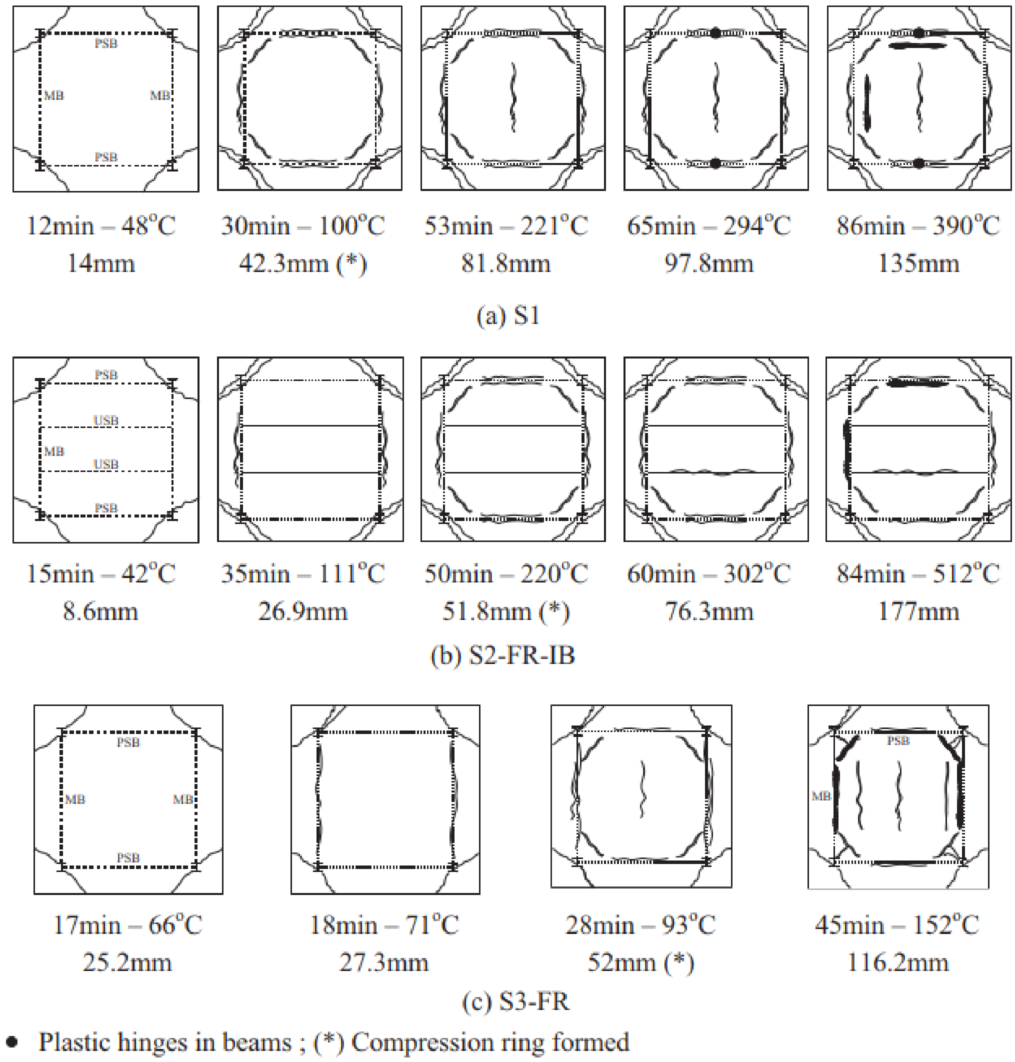

Fig. 17. Development of cracking pattern in specimens S1 through S3-FR [42]

This experiment was performed on ¼ scale specimens and so temperatures may not be representative of real construction. Nonetheless, this experiment offered a unique insight into the behaviour of composite construction where edge restraints were realistically simulated, and it was particularly useful to look at the effect of TMA on the development of the time-displacement history of the columns vertically and laterally. Column lateral displacements are a particularly important metric to appraise the performance of composite slabs in fire as they provide insight into the magnitude and direction of tractions developed in the floors and how they would impact, and be impacted by, the surrounding structure.

3.5. Tongji Composite Floor Tests

Li et al. [20] tested four full-scale arrangements of composite slabs on steel beams subjected to the ISO Standard Fire at Tongji University and published their results in 2017. The overall dimensions of the slabs were 5.2 m × 3.7 m with a 146 mm thick section consisting of 70 mm normal weight concrete on 76 mm deep 1 mm thick steel decking. An anti-cracking mesh with 8 mm diameter and 150 mm ×

150 mm spacing was installed with a cover distance of 21 mm or 30 mm from the top face of the slab. The slabs were connected to the steel framing with welded 16 mm diameter, 125 mm long shear studs placed 80 mm apart. Both primary and secondary beams were hot-rolled I-beams that were connected by high strength friction bolts fixed to full-depth welded plates. Three primary aspects of composite floor construction were investigated: the effect of presence or absence of an unprotected secondary composite beam, consequence of changing rib orientation, and outcome of changing the location of the reinforcement. The ribs were normal to the secondary beams in specimens S-1 and S-2 and parallel to the secondary beams for S-3 and S-4. S-1. Details of the various specimens are given in Table 4.

Table 4. Specimen information for the Tongji University tests [20]

Specimen	Concrete cover (mm)	Secondary beam?	Rib orientation	Mechanical load (kN/m^2)	Load ratio	Fire duration
S-1	21	Yes	Long-direction	18.4	0.6	75
S-2	30	Yes		17.7	0.6	90
S-3	30	No	Short-direction	8.8	0.6	100
S-4	30	No		9.5	0.65	100

The furnace used to test the slabs had a footprint of only 4.5 m × 3 m, and so only the slab and secondary beam were subjected to the ISO 834 fire. The primary edge beams were outside the furnace and bolted to its base frame to provide vertical, lateral, and rotational support. The rebars of the slab were extended by 150 mm beyond the slab edge to simulate edge continuity. The mechanical load was applied at 24 equally distributed loading points at 10% increments until reaching the testing load at which mechanical load was kept constant and thermal loading was started. The testing load corresponded to a fixed load ratio of applied to design load resistance of 0.6, with the applied loads given in Table 4. After application of the thermal load for between 75 and 100 min, a natural cooling phase was allowed with deflection and temperature recorders still in operation.

Despite S-1 being subjected to fire to only 75 min compared to 90, 100 and 100 min for S-2, S-3, and S-4 respectively, the maximum temperature measured at its surface of 874 °C was within 4% of the average surface temperature of slabs S-3 and S-4 which was about 911 °C. The reinforcement bars temperatures, however, were significantly different. The peak reinforcement temperature in S-1 was about 202 °C, while it was an average of 388 °C for S-3 and S-4. The large difference in reinforcement temperature was due to the shorter fire duration for S-1, and the higher distance of its reinforcement from the heated surface. Peak temperature was achieved in all specimens well into the cooling phase, which the authors note indicates the potential for post-fire collapse of composite floors due to continuously increasing reinforcement temperatures. Li et al. [20] also note that the temperatures in the concrete above the secondary beam are significantly lower than other areas in the slab due to the shielding effect of the beam.

The final deflections as a ratio of the length of the short direction of the tested slabs were $L/19$ and $L/20$ for S-1 and S-2 respectively, and $L/25$ for S-3 and S-4. Three reasons were given by the authors for the higher deflection of the slabs with the secondary beams (S-1 and S-2): (1) Despite being loaded to the same load ratio, S-1 and S-2 were subjected to nearly double the mechanical load of S-3 and S-4. (2) In specimens S-3 and S-4 where the ribs were aligned in the short direction better fire protection is provided by the concrete. (3) The temperature in the short-direction reinforcement in S-3 and S-4 was lower than those in S-1 and S-2, and short-direction reinforcement is a significantly more important contributor to membrane action [20]. These reasons are acceptable, except that as aforementioned, the average temperature in the reinforcement of S-3 and S-4 were almost double those in the reinforcement of S-1.

Another potential reason for the larger deflection of S-1 and S-2 is that the compositeness of the secondary beam coupled with the rigid boundary conditions results in a large gradient between the temperatures of the hot secondary beam and the relatively cold concrete. Furthermore, the separation of the slab into two panels supported on the secondary beam and restraining the thermal expansion at the edges resulted in negative moments on top of the secondary beam, and the development of large cracks there, as noted by the Li et al. [20] and shown in Fig. 18. These cracks, coupled with the diminishing capacity of the secondary beam to support the slab result in weakening the potential tensile membrane action at high temperatures.

It is immediately obvious that the compressive ring crack pattern was present in S-3 and S-4 indicating the development of TMA. The cracking pattern for S-1 and S-2 appear slightly different with diagonal cracks forming at the corners instead of the compressive ring cracks.

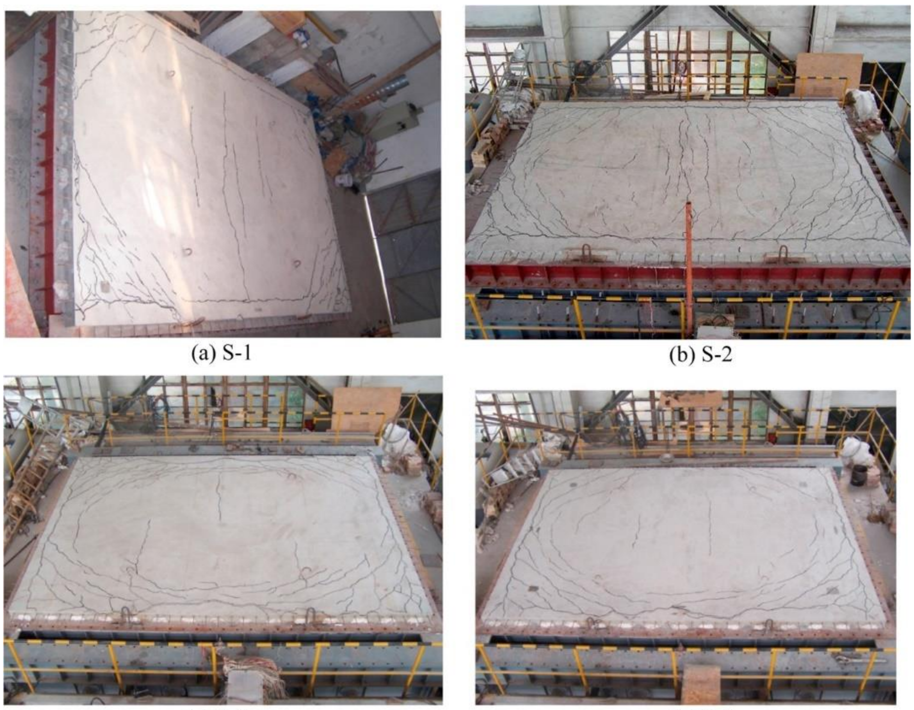

(a) S-1 (b) S-2

(c) S-3 (d) S-4

Fig. 18. cracking patterns observed in all specimens of the Tongji University tests [20]

According to Li et al. [20], the central crack in S-1 and S-2 facilitated heat transfer to the top of the slab by providing channels for convective heat transfer. However, it is not known how this interacted with the lower temperatures in the reinforcement achieved due to the shielding effect of the secondary beam at the same location. Cracks parallel to the supporting edge beams formed in all specimens, also due to the hogging moment at these locations. These cracks were more prominent along the direction of the ribs as shown in the figure. Li et al. [20] observed no bond slip in the reinforcement but did note that debonding of the steel deck did occur. It is not known how the rebar bond was monitored, however, as no measurements were presented for the rebar overhangs. Only a photo with significant cracking between the rebars is shown with the cracks delegated to the "pull-out trend" of the steel bars.

The Li et al. [20] experimental work offers important insight into the behaviour of restrained composite slab systems. Unlike the simply supported slabs tested in Lim and Wade [23], no diagonal cracks formed from the corners to the centre and the yield line cracking pattern was not observed. Large deformations did occur, and the compressive ring was clearer when the secondary beam was absent. The direction of the ribs and the presence or absence of the unprotected secondary beam has had a demonstrable effect on the results. Unexpectedly, the presence of the secondary beam appears to have exacerbated the deflections, although it must be noted that the mechanical load the slab was subjected to was almost double the slabs without the secondary beams.

4. Large Scale Tests

In this review, 'large scale tests' refer to experimental work performed on multi-span floors tested as a part of an overall structure. Therefore, while FRACOF and COSSFIRE were tests performed on a realistically sized structural assembly, they do not fit in this section because they only consisted for a single span without edge continuity. The two experimental programme that will discussed in this section cover a multi-span parking structure [44], and a three-storeyed building [45]. The two tests have significantly different thermal exposures, but both provide valuable insight into the system-level behaviour of composite floors in fire.

4.1. CTICM, ARBED and TNO Parking Structure

Zhao and Kruppa [44] reported on a large scale experiment performed on a purpose-built car park consisting of unprotected steel columns and beams supporting a steel-concrete composite roof. The test was an international collaboration between CTICM, ARBED, and TNO, with the results reported here published in 2004. The composite slab consisted of 40 mm deep dove-tail corrugated steel sheeting supporting a 120 mm thick slab. The car park had three 5 m bays and two 16 m bays, supported on 12 columns as shown in Fig. 19 (a). The structure was open to the outside air from all sides and had a 3 m storey height. The structure was subjected to two tests each of which consisted of exposure to the fire of a burning vehicle and differing only in the position of the burning car.

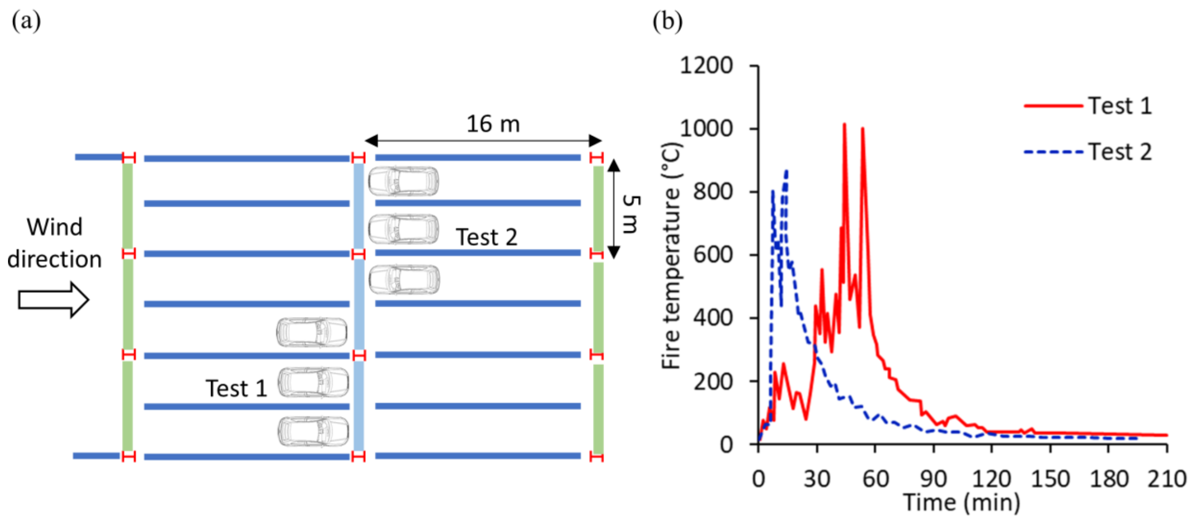

Fig. 19. The test by Zhao and Kruppa [44] (a) Plan of the car park (b) Gas temperatures for test 1 and 2

The magnitude of mechanical loading applied was not specified. The thermal load was applied by igniting the middle of the three cars parked on the ground floor and then letting the fire develop fully and spread to the adjacent vehicles. In the first test, the wind was blowing through the structure and against the rear of the ignited vehicle. This resulted in blowing the fire away from the body of the car and delaying fire spread. Peak temperature was reached between about 45 and 60 min from initial ignition and reduced to below 200 °C at around the 75-minute mark. In test 2, the wind was blowing against the front of the cars thus driving the flame into the rest of the automobile speeding the fire development and spread. Maximum gas temperature was reached in this test between 10 and 20 min from the ignition of the fire. The fire decayed relatively quickly with gas temperatures dipping below 200 °C after about 35 min. In both tests, the fire spread to all three adjacent vehicles and peak temperatures were sustained for only a short interval as shown in Fig. 19 (b).

The observed temperatures reached in only two locations were presented for each test. For both tests, the maximum temperatures reached in the secondary and primary beams were between 600 °C and 700 °C. The resulting deflections observed in test 2 were significantly higher than in test 1. During heating, they reached nearly 150 mm and then reversed their deflection during cooling and reached an upward deflection of nearly 50 mm. The deflections observed in test 1 reached a maximum downward deflection of about 65 mm and a maximum upward deflection of only 10 mm. Zhao and Kruppa [44] note that the effect of the wind on the development and spread of the flame was responsible for the difference in observed deflections. In test 2 the growth and spread of the fire were assisted by the wind which also pushed the flames towards the enclosed area of the structure. This resulted in a significantly larger heated area and thus larger deflections. In test 1, the wind direction had the opposite effect as it pushed the flames away from the structure and significantly reduced the severity of the fire.

Out of all experiments discussed in this chapter, this was the only one where a full-scale structure was subjected to a localised fire. Unfortunately, the information obtainable in English is limited to brief publications such as [44]. Not much is known about the deflections and temperatures observed in other parts of the structure other than those reported here. It was observed in the test that the deflections, even the most severe, were relatively small with a deflection to short span ratio of about L/33. No significant local failures were reported, and the overall structure remained stable. Bolt rupture during the cooling phase was noted at the lower part of the rigid beam-column connection. Despite this localised failure, the integrities of the overall connection and the structure were not compromised.

4.2. Shandong Jianzhu University Composite Building

The experiment performed at Shandong Jianzhu University in Jinan, China is the largest since Cardington and included four large-scale tests and was published in 2013. A nine-meter high three-storey steel-framed building with composite flat reinforced concrete slabs was erected and tested under mechanical and fire loads [45–47]. The building had a 13.5 m × 13.5 m footprint divided over three 4.5 m bays in each direction. The floor framing consisted of H 250×125×6×9 beams, while the columns were H200×200×8×12 sections. The framing is reported as being of the Q345 grade in the first two tests [46], and of the Q235 grade in the other two [45, 47].

The flat slab was 120 mm thick, and bottom-reinforced with 8 mm rebars in a 125 mm × 125 mm grid with various top slab reinforcement provided around the floor framing. Concrete cover was 15 mm and 20 mm as reported in [46] and [45, 47] respectively. The concrete used was normal weight with a compressive strength of 33.8 MPa on the day of the test [46]. Composite action between the slab and beams was achieved by using 16 mm diameter headed shear studs placed 200 mm apart atop the web of the steel beams. Moment connections between the beams and columns utilised a beam stub welded onto the columns and then connected to the floor framing with bolted plates. All floor framing was protected from heating and kept outside the furnace walls in tests 1 and 2, while only the connections, columns and perimeter framing were protected in tests 3 and 4.

The fifty kg sandbags were used to apply a uniform mechanical load of 2 kN/m^2. Test 1 was performed to assess the behaviour of a corner slab, while Test 2 was performed on an internal panel on the top floor of the tested building. Tests 3 and 4 were performed on four and six bays, respectively, and aimed to study the impact of more realistic and substantial fire exposure. The differences between the four tests are summarised in Table 5.

Table 5. The main differences between the four Shandong Jianzhu University tests

Test	Floor	No. of exposed panels	Heating time	Maximum gas temperature	Maximum unexposed surface temperature	Maximum deflection
Test 1 [46]	Roof	1	270 min	885 °C	226 °C	142 mm
Test 2 [46]	Roof	1	306 min	897 °C	242 °C	114 mm
Test 3 [45]	3rd	4	290 min	851 °C	180 °C	180 mm
Test 4 [47]	2nd	6	225 min	794 °C	229 °C	148 mm

The furnace temperatures in all tests did not follow a standard temperature-time curve, and the criteria for furnace shut off was not explained. In all cases, the heating phase lasted well in excess of three hours and the total test time was fifteen and ten hours for the first and second tests, and the third and fourth tests, respectively. For tests 1 and 2, the temperatures reached between 300 °C and 500 °C and then climbed up to nearly 900 °C over the next five hours [46]. The gas temperatures were slightly lower for tests 3 and 4 because the furnace area was significantly larger than the previous tests, and because some of the 16 oil burners used failed during the tests. According to the authors' of the Shandong Jianzhu University studies, controlling the burners was a particularly challenging aspect of performing the large-scale tests and resulted in the low heating rate applied to the structure [47].

The maximum recorded temperature and heating duration for each test is summarised in Table 5. The moisture content of the concrete was about 2.3% and resulted in a plateau in slab temperatures at 100 °C that was clear and consistent across all tests. Despite the significant moisture content, no spalling was observed in any of the tests which Li et al. [47] note may be a result of the low heating rate. The temperature during the heating phase at the top of the concrete slab reached a maximum of 187 °C and 217 °C in tests 1 and 2, respectively, but continued to increase during the cooling phase. The maximum temperatures in the top of the slabs were reached during the cooling phase in all tests, and are shown in Table 5.

The maximum recorded central deflections in tests 1 and 2 were 142 mm and 114 mm respectively, which corresponds to $L/32$ and $L/40$ respectively. Tests 3 and 4 naturally had higher deflections with a maximum deflection ratio of $L/25$ reached in Test 3. The deflected shape of the panel in Test 1 was distinctly unsymmetrical, which was caused by two large cracks appearing around the quarter-point away from the interior edges. The deflections recorded in the transducers adjacent to these edges just outside the cracked zone had a maximum deflection of 67.2 mm. According to Yang et al. [46], the severe cracking parallel to the interior edges resulted in releasing the stresses and significantly lowering the rotational restraint beyond the crack and away from the interior edges. The maximum deflection should then be at a point between the large cracks and the centre of the panel.

In Test 2, the vertical deflections were largely symmetrical with the maximum deflection occurring at the centre of the slab. The deflection patterns are not as clear in tests 3 and 4, and are difficult to judge fairly as the thermal exposure conditions within the compartment were complex due to the heating method used. Observation of the horizontal displacements also reveals that the edges of the panels in Test 1 were first pushed out, and then were pulled in because of thermal expansion and the large deflections in the slab, respectively. The lateral deflections for Test 3 paint a different picture where the lateral deflections are always expansive during the heating phase. At a similar location (middle of outer edge of a panel) in test 4, the lateral deflections were non-existent, and instead the displacement at an adjacent column was contractive. Explanations were offered in all these cases [45–47], but when considering the big picture and looking at the four tests, it becomes apparent that the stress-state and tractions within the slab are more complicated than what engineering intuition would reveal at first inspection.

Fig. 20 showcases the damaged state of the panels of all tests. The patterns observed in tests 1 and 2 are particularly insightful as the cracks extended beyond the fire compartment and into the adjacent structure. The first crack to appear in Test 1, and the second to appear in Test 2, was an edge crack parallel to the support beam at the inside of the interior edge of the heated panel. This crack likely occurred due to restrained hogging moments enforced by continuity of the floor slab. Similar cracks appeared on the other interior edge in Test 1, and on all edges of the panel in Test 2. Cracks parallel to the edges also appeared in the panels demarking the well-documented compression ring. For Test 1, however, these cracks occurred only parallel to the interior edges and not parallel to the exterior edges. Cracks diagonal to the column occurred instead, as shown in Fig. 20 (a). Two large cracks denoted 5 and 6 in the figure also appeared in test 1 and reduced the moment constraint significantly affecting the deflected shape as discussed earlier.

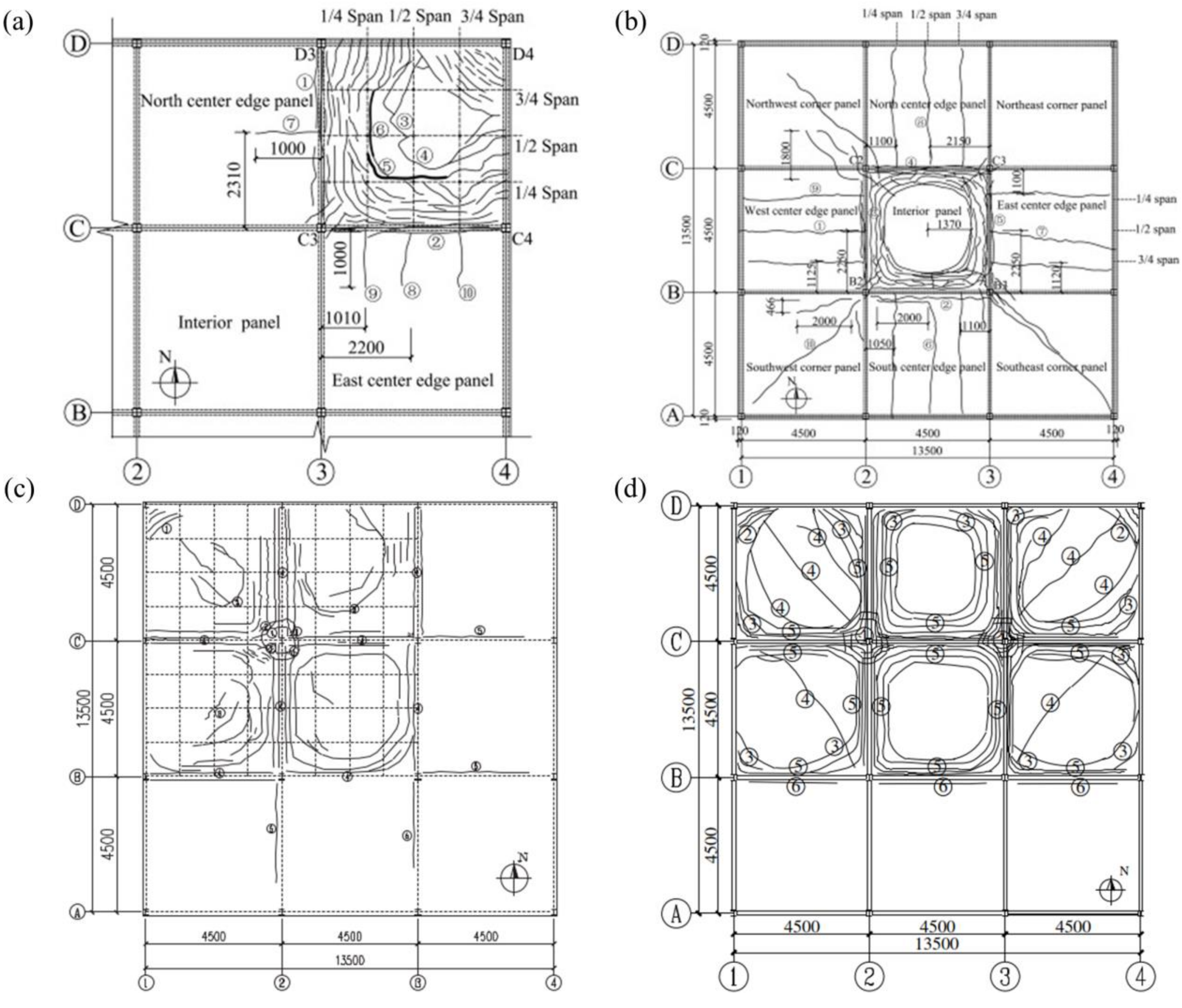

Fig. 20. Cracks developed in (a) Test 1, (b) Test 2, (c) Test 3, and (d) Test 4 [45–47]

In Test 2, long cracks normal to the edges appeared and crossed all adjacent panels as shown in Fig. 20 (b). Yang et al. [46] attributed these cracks to the restrained sagging of the unheated panels induced by the effect of the supporting beams and slab continuity, which would result in tensile stresses in the unheated panels. If that were the case, however, then the cracks on the unheated panels should have been parallel to the edges of the heated panel and not normal to it as was observed.

The observed direction of the cracks indicates that tensile forces were generated tangentially around the heated slabs, which may have occurred simply due to its in-plane thermal expansion. As the central panel expands laterally, it generates compressive forces normal to its edges and its expansion would be resisted by tensile forces parallel to its edges. This would cause the observed cracks to open early in the heating phase, as was the case with crack 1 in Fig. 20 (b) which was visible after only 4 min from the ignition. All other cracks in the unheated panels started to form within the first 52 min of the fire, further pointing to this mechanism. The diagonal cracks likely occurred to accommodate the tensile stresses accompanying the diagonal compressive struts caused by the expansion of the central bay.

The visible cracks in Test 3 are shown in Fig. 20 (c). Despite a significantly larger area of the floor being exposed to thermal load, the cracks appear to be highly localised within the heated region unlike the observations made in Tests 1 and 2. Likewise, very minimal cracking is observed outside the heated region for Test 4 as depicted in Fig. 20 (d). The cracking of the individual panels is governed by their location within the floor plate and the amount of available restraint. However, it is surprising that further damage to the surrounding structure did not occur especially considering the severity of the exposure and comparing the observed damage in tests 3 and 4 with the damage observed in Test 2.

The experiment reported by Yang et al. [46] provides particularly unique insight into the effects of slab continuity, and the impact of edge restraint conditions as provided by the adjacent structure or lack thereof. Despite the unrealistically long heating regime, the slab still sustained a significant gradient and the compression ring, or part of it in the case of test 1, were observed. The additional restraint of the interior panel of test 2 indeed afforded it more stiffness resulting in lower deflection compared to the corner panel of test 1 which suffered from significant cracking within its span that negatively impacted its deflected shape. The deflected shape in the corner panel test was, therefore, unsymmetrical. Cracking in the unheated panels in test 2 was very significant and extended to the edge of the building.

In all cases, however, edge parallel cracks due to hogging moments were observed and point to the importance of considering realistic boundary conditions when analysing floor plates in fire. The inclusion of further panels and exposure of a larger floor area to fire in test 3 and 4 provides additional data to consider. The complexity of the thermal conditions within the massive furnaces that were constructed, and the lack of extensive lateral-movement instrumentation and inconsistency in the results of the available lateral measurement results make the results of these two tests challenging to decipher. The localised cracking patterns in the large tests are also surprising considering that the significantly less severe Test 2 caused extensive damage in the entire floor plate. As the authors of the Shandong

Jianzhu University studies note, there is a pressing need to study the experiment in further detail to truly utilise the abundant data it provides.

5. Theoretical Approaches for Analysis and Design

The coalescence of the generated knowledge on the behaviour of composite slabs in fire into a simple but effective design method is a natural progression and aim of many of the afore-discussed experimental investigations. Understanding the failure mechanisms adopted within these methods is important for designing the integrated simulation environment to capture the kind of behaviour expected. It is hoped that the theoretical methods presented would also provide insight into the possible failure mechanisms of the WTC7 composite floors. From the first studies on Cardington, the methods diverged into two distinct branches: Yield Line methods, and other methods. All the methods to be discussed in this section share the assumption that designing a slab as simply supported without lateral edge restraint produces a conservative design which predicted capacity would be outperformed by the strength of a real slab in a fire or experiment.

All the methods also assume that a composite slab on corrugated steel decking could be treated, also conservatively, as a flat, lightly reinforced slab with all effects of the steel decking ignored. The steel decking is always neglected because of observation during the Broadgate, Basingstoke, and some experiments. It is postulated that the steam from the concrete would result in delamination of the decking, and that the thermal exposure would cause rapid loss of its mechanical strength. Furthermore, none of the methods discussed considers finite shear slip between the composite beam secondary beam and the slab, or the edge beams and the slab. None of the methods considers the reaction of the slab during cooling, either. Most methods, such as Usmani and Cameron's method [48], assume that failure during cooling is likely to be avoided if sufficient capacity during heating was provided and if connections were designed with sufficient ductility at ambient conditions.

5.1. Yield Line Methods

5.1.1. Bailey's Method

The yield line-based methods originated in 1943 [49] with the publication of the original method in Swedish in Denmark, followed by further development by others [50–53]. A thoroughly detailed historical background to the origins of the yield line method can be found in [54], which eloquently describes the method and its history from Johansen [49], to Hayes [52, 53] and Bailey [55]. Bailey and Moore [56, 57] were amongst the first to use the yield line method for application to composite and flat slabs subject to fire. Bailey further popularised the method via numerous publications in almost every relevant journal e.g. [6, 25, 33, 58], and calibrated and validated the method against many experimental tests such as those described in the previous section [25]. The method was also adapted and extended by the Heavy Engineering Research Association (HERA) for the slab panel design approach [59, 60].

Bailey's method, as it will be referred to in this section, begins with the yield line pattern shown in Fig. 21 (a) that would form as a slab resisted transverse loading in bending. The yield lines demarcate the locations at which the reinforcement would yield in flexure and around which the assumed-rigid slab segments would rotate. It is by considering the equilibrium of the forces within these segments and enhancing them with the contribution of membrane stresses that a capacity would be found for a given deflection, which is empirically limited to a conservative value.

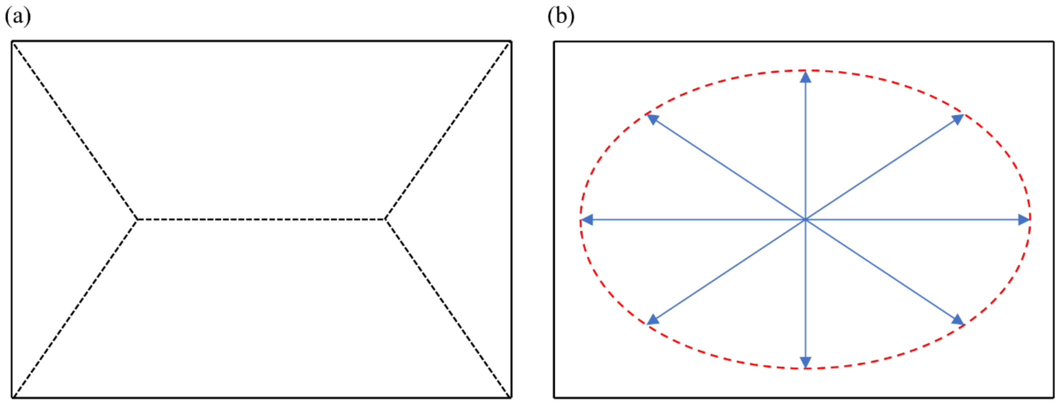

Fig. 21. load-carrying mechanisms of simply supported slabs (a) yield line, and (b) tensile membrane action supported on compressive ring

Failure is expected to occur in one of two forms: in the middle of the slab with a through-depth crack forming along the short direction and reinforcement rupturing there, or compressive fracture of the concrete along the compressive "ring" which occurs to balance out the tensile membrane action occurring within the central region of the slab as shown in Fig. 21 (b). Despite its prominence and application in practice [61], the Bailey method is subject to numerous criticisms from within the research community. Many of the methods discussed next were developed to compensate for some shortcomings in Bailey's method [62] or to replace it with a more physically consistent approach [63].

5.1.2. The Flexible Edge Model

Nguyen and Tan demonstrated that the assumption of rigid vertical edge support is moot because the edge beams, even with protection, deflect significantly [61]. They also suggested that by considering the secondary beam as composite with the slab, Bailey's method effectively double-counts the contribution of the concrete flange of the composite beam [61]. Indeed, the experiments by Nguyen and Tan [61] demonstrated that the Bailey method overestimated the tested floor systems capacity by an average of 11% including a 2.28 times overestimate in the capacity of the secondary beams. The assumption of an over-predicted load capacity was based on the actual failure deflection of the slabs, however, and not on the conservative deflection limit promoted by Bailey's method. When the authors applied the deflection limit of Bailey's method the results were once again within the bounds of the experimental capacities.

Nguyen and Toh's model [61] circumvents the issue with the deflected edge beams by considering their deformation within the framework of their model. Once enough deformation is achieved in the edge beams leading to their failure, a "folding mechanism" forms, tensile membrane action is lost, and the floor system would collapse. It is worth noting that this folding mechanism is assessed in Bailey's method [57] by rechecking the capacity of the edge beams after the membrane capacity is deemed sufficient, although the deflections of the edge beams are not considered when calculating the membrane enhancement. These deflections would indeed reduce the membrane enhancement as the relative displacement between the rigid segments and the edge is reduced lessening the contribution of the membrane forces to the overall resistance of the floor.

5.1.3. The Imperial Method

Another method that could be considered to loosely exist within the yoke of yield line methods is that developed by Omer et al. [64–66] and extended by Cashell et al. [27, 29] at Imperial College London. This method, referred to herein as the Imperial method, also assumes that the slab would deform following the kinematics prescribed by the Yield Line theory where distinct yield lines form along the slab surface and over which the remaining rigid segments can rotate but not break away from before ultimate failure. Similar to Bailey's method, this approach also assumes a specific distribution of stresses between the rigid segments but does not rely on enhancement factors to increase a flexural yield line-based capacity.

Moreover, despite assuming rigid rotations about the yield lines, the method also considers the effect of thermal gradient on each rigid segment, which is more compatible with experimental observations and something no other yield line-based method had done up to that point. Due to this, the method requires an iterative solution for each temperature level. Failure, according to [64], was only considered along the short-direction through-depth crack or two through-depth cracks at the intersection of the diagonal and horizontal yield lines over which the reinforcement would rupture. This was later extended with the inclusion for potential compressive failure along the compressive ring [29].

One of the primary contributions of the Imperial method is that it considers the concentration of strain in the reinforcement across the through-depth cracks and relegates the failure to the strain expected for rupture of the reinforcement at the crack locations. The bond strength between the rebars and the concrete is critical within this model, as the loss of bond at the location of cracks and its development up to its full strength away from the crack face or slab edge influences the strain in the rebar significantly and can thus affect the failure predictions. Cashell et al. [27] validated the model against tests at ambient temperature, and further studied the effect of the constitutive relationship of the reinforcing steel, reinforcement area, and geometric configuration of the slab. It was found that more ductile reinforcement is more likely to result in crushing failure of the concrete within the compressive ring, while less ductile reinforcement is likely to fail in tension.

One of the main drawbacks of this model is that it is highly influenced by bond strength assumptions, over which only little information is available in the literature. While this may hinder the direct application of the model in design and analysis, this ought not be considered a deficiency in the method but rather point towards its more holistic consideration of the behaviour of slabs at ultimate limit state and the many factors that can influence ultimate failure.

5.1.4. The Burgess Method

The latest addition to the library of analytical approaches for analysing and designing slabs to incorporate the additional capacity provided by tensile membrane action is provided by Burgess [67], Burgess and Sahin [68], and Burgess and Chan [62]. Starting with an ambient analytical method in 2017 [54], Burgess set the groundwork for his approach by doing away with the traditional practice of establishing equilibrium at the yield lines and focusing on the overall equilibrium of the system. This results in 30 different possible combinations of stress-block configurations associated with the changing inclination of the neutral axis on the concrete surface at the yield lines. The stress block eventually rises above the top surface of the slab leaving only the reinforcement in tension at the crack location. The Burgess method was extended for thermal action in [68] where the effect of reinforcement ductility and varying yield line pattern due to orthotropy of the floor system were also addressed. The Burgess method is fundamentally different from Bailey's method on multiple levels. First, Bailey's method prescribes a yield line pattern of a lightly reinforced concrete slab ignoring the inherit orthotropy of the composite floor system introduced by the direction in which the secondary composite beams act because of the assumption that at high temperatures the secondary beams would have lost most of their capacity. The Burgess method considers this orthotropy from the beginning because according to Brugess and Sahin [68] the yield lines would form at relatively low temperatures and once formed do not change, and are affected by orthotropy.

Finally, Burgess' method explicitly accounts for the change in concrete contact conditions and fracture of reinforcement in either and both directions across the yield lines, which would lead to eventual failure predictions that closely adhere to the physics of the collapse mechanism. Burgess and Chan [62] updated the method, although for ambient, to consider edge restraint. Their findings indicate that initially, compressive membrane action acts to increase the initial capacity, but is quickly lost at higher deflections of the slab. They also discovered that by considering lower-bond reinforcement such as plain rebars, the potential for enhancement due to tensile membrane action increases significantly due to larger deflections and increased crack width at which the reinforcement would rupture. These observations and their consideration remain to be included in fire in future iterations of the Burgess model.

5.2. Other Methods

5.2.1. Energy Method

Usmani and Cameron [48, 63, 69] believe that the yield line approach is incompatible with the deflections observed in real fires. According to their model, a composite slab at elevated temperatures takes the form of a sinusoidal curve in both lateral directions without any discrete discontinuities analogous to the yield line method. This assumption, which is in contradiction to all other yield line methods aforementioned, is based on numerous first-hand observations and numerical studies performed on the Cardington experiments [8, 70–72]. While the deflected shape is primarily induced by thermal strains, thermal forces and moments would develop within the slab due to restrained expansion. By assuming that failure occurs as the reinforcement reaches rupture strain as prescribed by Eurocode 2 [73], and by considering both the deflected shape and corresponding mechanical strain in the reinforcement, a deflection limit is set for each temperature considering thermal degradation of material. Since the deflected shape is a sinusoid, then each rebar would have a different strain and stress state, and this must be accounted for when calculating the internal energy which is the next step. The internal work needs to be calculated iteratively due to the nonlinear deflection response of the slab.

The final step would be calculating the external work, and equating it with the internal work to estimate the ultimate capacity of the slab that would result in rupture of the rebars at a given temperature. This procedure needs to be carried out for a number of temperature points to construct a temperature-deflection and temperature-load envelopes. Comparison with the Cardington experiments demonstrate close agreement with the calculated deflection and showed that most of the experiments had ample capacity to survive further heating and loading. The capacity of the internal secondary beams are not considered in the method, and as shown in Cameron and Usmani [69], even at 900°C the 6% remaining capacity of the secondary beams can be nonnegligible. The problem with calculating the secondary beam capacity at such high temperatures is that the response is highly nonlinear with small errors resulting in big differences in capacity estimates [69].

Another important finding that this method demonstrated is the importance of short span reinforcement. It was observed that for the same level of vertical deflection, compatibility requires the short span strain to be near double the long span strain. This is, of course, highly dependent on the aspect ratio of the slab panel analysed with the increase of which the accuracy of the Cameron-Usmani method decreases [69]. Finally, the anchorage of the tensile membrane action in this method ignores the stabilising effect of the compressive ring and transfers the lateral and torsional forces directly into the surrounding frame and its connections, with the cooling phase being most critical for the latter. Therefore, by following this method, designers must consider the additional forces that the rest of the structure would be subject to and design for capacity and ductility accordingly. The absence of torsional distortions in the perimeter girders of the Cardington experiment suggests that these capacities are implicitly included within standard design procedures for ambient conditions. Nonetheless, it is important to verify the surrounding structure is indeed capable of sustaining new load paths generated from tensile membrane action whenever that capacity is exploited for accidental damage design.

5.2.2. Variational Method

Abu et al. [74] approached the problem of estimating the tensile membrane action contribution to fire resistance from a computational mechanics point of view by relying on the Rayleigh-Ritz method with prescribed shape functions. First, the differential equation governing the large deformation of an elastic plate is established alongside its boundary conditions. The boundary conditions assumed no lateral force, moment, vertical deflection, or curvature in either direction at the slab edges. Then, a linear thermal gradient is assumed through the depth of the slab along its corresponding mechanical strains. With this information established, the internal strain energy is calculated by prescribing a number of shape functions to describe and relate the freedoms of the problem and integrating over them.

Based on this Rayleigh-Ritz approach, Abu et al. [74] established that tensile membrane action can be achieved with thermal gradient alone, and can successfully support itself via a compressive ring without requiring lateral restraint as vertical restraint is sufficient. For accurate prediction of stresses especially along the boundaries, however, the method would require a large number of shape functions for which minimizing the total potential energy becomes more and more computationally expensive, and with no guarantee that the result would be significantly more accurate. While the usefulness of this model lies in assessing the feasibility of phenomenon such as compressive ring supporting tensile membrane action, it is not expected that it can be practically used by engineers for analysis or designs, which was not the intention behind developing this model in the first place.

5.2.3. Elliptical Membrane Model

Li et al's [75] and more recently Zhang and Li's [76] models are based on observation of slab behaviour during fire. While these models assert that in the early stages of a fire the slab resists its loading primarily in bending, they assume that the yield line would disappear as the load resistance mechanism transitions into tensile membrane action at high temperatures. As temperatures continue to grow, the yield lines would form due to the thermal degradation of stiffness. At even higher temperatures, however, the load-carrying mechanism changes from bending into an elliptical central tensile membrane region surrounded by a compressive concrete ring. The approach is relatively straightforward. First, the slab is considered to consist of four rigid segments that comprise the concrete compression ring as shown in Fig. 22.

Failure is assumed to occur when the reinforcement ruptures, or the concrete ring crushes. The limit on rupture of the reinforcement is set by calculating an ultimate deflection accounting for the rigid rotation of the ring segments based on yield line theory, and a deflection of the elliptical segment at which the reinforcement would reach rupture strain. The ultimate capacity can then be calculated by taking force and moment equilibrium over the ring segments and considering the capacity of the elliptical segment. Assessment of concrete crushing in the ring is carried out as a simple capacity check after the ultimate rupture capacity is established. The 2010 version of this model provides a simpler way to calculate the forces at the boundaries and ensures equilibrium within the slab.

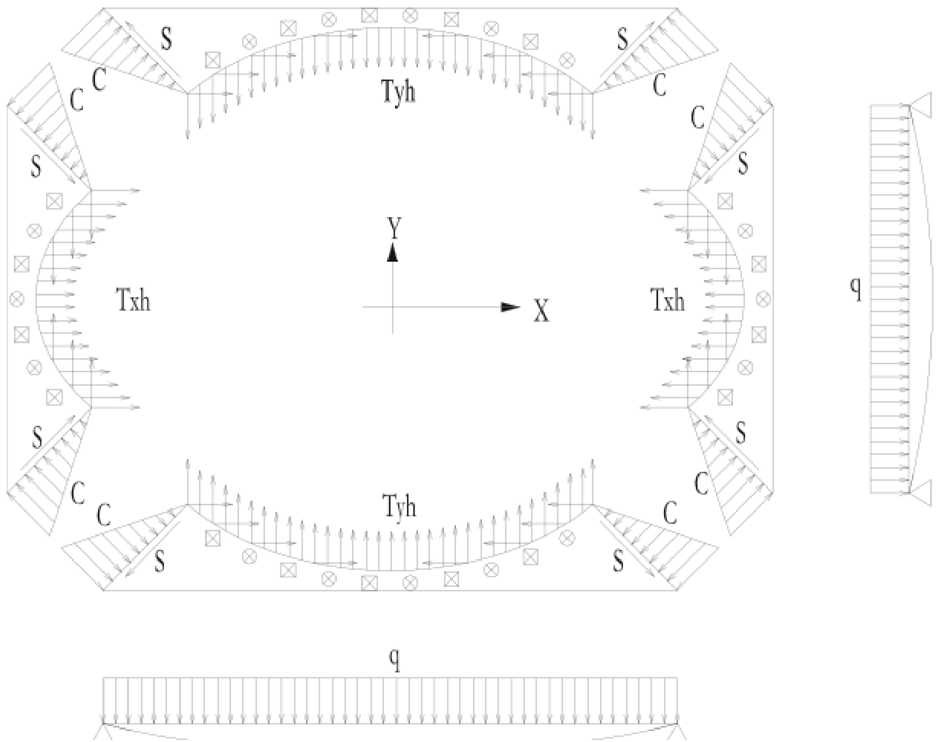

Fig. 22. Zhang & Li's model representation of the compressive ring and tensile region [76]

The validation of the model provided in Zhang and Li [76] compares experimental values against Bailey's method, the older version of the model [75] and the 2010 model. Unfortunately, the 9 results shown in the validation suggest that the 2010 model is likely to significantly overestimate the capacity of the slabs, which is something that the results predicted by Bailey's model and the 2007 model do not do. Indeed, the validation results in [76] suggest that the 2007 model [75] is significantly better at predicting safe results. However, this observation is based on only nine validation data points provided in [76], which is far below a sufficient number of observations for achieving statistical confidence.

6. Discussion

In this paper, several recent experimental and theoretical studies on the behaviour of composite floors in fire were presented. Through this literature review, it is apparent that the current understanding of the behaviour of composite slabs in fire is largely based on extrapolation from a limited number of idealised tests on a relatively small number of specimens which are summarised in Table 6. All major experimental work, except for the CTICM, ARBED and TNO Parking Structure [44], was based on highly idealised temperature-time curves such as the ISO 834 or arbitrary heating rates enforced by logistical considerations.

Table 6. Summary of surveyed experimental studies

Experiment	Fire	Scale	boundary	Test description
BRANZ Slab Tests [23]	ISO 834	Full scale; 3.3 m × 4.3 m	Simply supported with clamped corners in some specimens	6 NWC flat slabs with different reinforcements loaded uniformly and heated in furnace for 3 h
University of Manchester Small Scale Tests [25]	Ambient; 300 °C/h up to 1000 °C	Small scale; 1.2 m × 1.2 m and 1.8 m × 1.2 m	Simply supported with clamped corners	44 NWC (assumed) flat slabs with different reinforcement types; half tested at ambient until failure and half tested at elevated temperature
University of Sheffield Small Scale Tests [18, 19]	Electric kiln, unspecified	Small scale; 0.6 m × 0.6 m, 0.92 m × 0.52 m, 0.9 m × 0.5 m	Simply supported with clamped corners	38 NWC flat slabs with either plain or deformed reinforcement with different reinforcement ratios
Imperial College Tests [28]	Ambient	Small scale; 1.7 m × 1.7 m and 2.45 m × 1.7 m	18 simply supported, 2 fully restrained	20 NWC (assumed) flat and ribbed slabs with different reinforcement types, ratios, and depth. Tested at ambient until failure under uniform load
SEU Profiled Slab tests [32]	ISO 834	Full scale; 3 m × 1.86 m	Edge embedded into large concrete beams	2 NWC (assumed) ribbed slabs composite with steel deck loaded uniformly and heated for 90 min. Very weak concrete so early cracking
BRE Large Slab [33]	Ambient	Full scale; 9.5 m × 6.5 m	Attached to supporting steel frame with shear connectors along edges	LWC ribbed slab stripped from steel decking and loaded uniformly until failure in TMA by reinforcement rupture
The Michigan State Composite Floor [21]	ASTM E119	Scaled frame, full scale slab; 3.96 m × 2.13 m	Slab extends beyond framing; no explanation of connection to furnace	3 LWC slab on trapezoidal steel deck partially composite with two girders connected by three secondary beams
FRACOF & COSSFIRE [16, 17]	ISO 834	Full scale structural assembly, 6.66 m × 8.735 m and 6.66 m × 9.0 m	Slabs composite with steel frame using headed shear studs	2 tests on NWC ribbed slabs on trapezoidal deck composite with steel frame of different arrangement and fire protection subject to 120 min of heating
NTU Scaled Composite Floor Tests [42]	20 °C/h up to 800 – 1000 °C	Small scale; 2.25 m × 2.25 m	Finite restraint for rotational and in-plane movement	8 NWC (assumed) flat slabs composite with edge beams and internal secondary beams uniformly loaded and heated up to 2 h
Tongji University Composite Floor Tests [20]	ISO 834	Full scale; 5.2 m × 3.7 m	Edge steel frame fixed to furnace support beams	4 NWC slabs on trapezoidal steel deck fully composite with steel frame uniformly loaded and heated for up to 100 min
CTICM, ARBED and TNO Parking Structure [44]	Real car fire	Full scale structure, 32 m × 15 m open air car park	Slabs composite with steel framing using shear studs (assumed)	2 test fires in an open car park
Shandong Jianzhu University Three-floored Composite Building [45–47]	Gentle 5-h fire	Full scale building, 13.5 m × 13.5 m	Slab composite with steel framing using shear studs; one central test and one corner test	4 tests in a NWC flat slab composite with primary steel frame in a 3-floor building

Almost all theoretical methods developed so far assume that the simply supported boundary condition is the most critical in a fire. Therefore, Bailey's yield line approach and its extensions all rely on the development of a clear yield line pattern which only seems to occur in select experiments without strong edge restraints, and particularly in tests performed at ambient such as [28, 33]. So far, there does not seem to be strong evidence that a real slab subjected to fire would deflect according to the discretised-segment model adopted in Bailey's method. What was observed in most experiments is cracking at locations which are subject to high levels of restraint such as slab corners [16, 17, 20, 32, 40–42], and the proximity of edge beams [16, 17, 20, 21, 40, 42, 46]. There was also a less frequent observation of cracking through the depth of the continuous portion of a composite slab on steel decking [20, 21, 23, 46]; an outcome that was not reported to have presented in COSSFIRE and FRACOF [16, 17]. Likewise, cracking over secondary beams was reported in [20, 21, 40–42], but not in [16, 17].

Furthermore, experiments such as the BRE Large Slab [33] and the Imperial College Tests [28] strip their slabs from the steel deck to perform ambient-temperature tests. This is because steel decks are assumed to buckle, debond, and lose strength in fire quickly. Debonding was indeed observed in [20, 23], but was not noted to have occurred extensively in [16, 17, 21]. Despite the observed local debonding of steel decking in some tests it may still contribute at least to the early stages of fire where it may still retain a portion of its strength. This effect should be significantly more prominent in more realistic fire exposure conditions where temperatures may not exceed 700-800 °C for a short duration such as in the parking structure tests [44], and where the steel deck is fully protected as was the case in WTC7 [9]. The shear connectors between the beams and slab were not observed to fail in most tests, without any observed failure. Likewise, all beam-beam and beam-column connections survived the fire tests without runaway failure including the unprotected connections of COSSFIRE [17].

6.1. Challenges and Needs of Future Research

There remains a multitude of areas ripe for exploration as the work of previous researchers has generated a number of research questions that need to be addressed in the future.

6.1.1. Effect of slab continuity in composite floors

Considering the experiments reviewed, it is clear that most were highly idealised and are distinct from realistically complex construction and modern architecture. Furthermore, almost all experiments focused on idealised single panels disjointed from any adjacent structural elements that would be present in any real building. When larger experiments were carried out, such as the full-scale experiment at Shandong Jianzhu University [45–47], the floor system behaviour became significantly more nuanced. Varying top and bottom reinforcement and the continuation of floor slab over multiple bays are key factors in producing non-localised cracking patterns such as those shown in Fig. 20 and are outside the scope of a single panel experiment.

The CTICM, ARBED and TNO Parking Structure [44] also demonstrated that fire may cause alternating sagging and hogging of adjacent spans due to slab continuity. This may cause premature cracking in the top concrete layer of the unheated span, and depending on the stiffness of the slab panel and the severity of the exposure could result in failure at the interface between the panels as shown in the NTU tests [40–42]. This is important not only for the ultimate limit state, but also for serviceability and repair of fire-damaged structures: repair may become necessary even away from the fire exposed panel. Further work needs to investigate the effects of continuity on composite floors to characterise these behaviours and more robustly capture the effect of finite restraint.

6.1.2. Impact of moderate fire exposure

The most common approach for performing structural fire tests relies on subjecting the structural components to the maximum reasonable fire exposure which often is the standard temperature-time curve. This assumes that the ultimate limit state is the performance level being designed for and that the primary consideration is failure avoidance. While this is a valid assumption, there is also a need for studying the behaviour and damage-accumulation of composite slabs exposed to moderate fires. Moderate fires are far more likely than worst-case scenario fires and are responsible for the majority of repair costs [77]. The only tests that studied the structural response of buildings subject to moderate and real fires were the Zhao and Kruppa parking tests [44].

The results of these tests showed that even with this exposure a localised connection failure did occur which indicates that even localised moderate fire exposure may affect structural integrity and could necessitate significant structural repair. The effect on the concrete and both the structural and thermal integrity of the slabs after the fire were not discussed in detail in that work, however. Future work should clearly measure and record the damage in the composite slab such as crack patterns, widths, and the damage-state of the reinforcement and steel decking.

6.1.3. The role of steel decking in fire resistance

The steel decking acts as the tensile reinforcement for composite slabs under ambient conditions but has been assumed to quickly lose capacity and debond in the case of fire. This assumption held true in the BRANZ slab tests [23] and in the Tongji University composite floor tests [20] but was not reported upon in COSSFIRE or in the Michigan State University Tests [21, 35]. Furthermore, the role of embossments on the debonding in fire has not been extensively studied particularly in multi-panel floors. The continuity of the decking over multiple panels may potentially result in better two-way structural performance in fire and this should be investigated in the future.

6.1.4. Quantification of the effect of edge torsional restraint

The design methods discussed assume that torsional restraint will be sufficiently provided by edge beams. However, the quantification of this torsional boundary condition is still an open problem when considering the impact of through-thickness cracking over the edge beams and how that may affect compositeness. Research focusing on the thermal effects on the torsional stiffness and ultimate capacity of edge beams is still needed.

6.1.5. Establishing new failure criteria for composite floors in fire

The current collapse criteria for composite floors subject to fire are inadequate. As seen in the experiments presented, composite floors could reach deflection to short span ratios of up to $L/9.3$ at failure, which exceeds the $L/20$ deflection criterion by a large margin. Furthermore, a common criticism of Bailey's method is that the failure criterion is empirical and requires further refinement [67]. Because of this, the failure criteria adopted by the experimental investigations reviewed were varied. Some, such as Wellman et al. [21], adhered to the $L/20$ or the $L/30$ with $L^2/9000$ deflection rate criteria. Others, such as the NTU team [40–42], opted for a more qualitative failure indication including the size of the crack at the edges of the slab. More representative rules for failure classification need to be developed for a more unified approach for the study of composite floors in fire, and for the design methods that aim to leverage the added capacity provided by TMA.

6.1.6. Clear definition of tensile membrane action

Despite TMA being the fundamental mechanism in which composite floors resist fire, it remains a vaguely defined mechanism. Currently, TMA is considered to have occurred based on qualitative observation of unquantified 'large deflections' and the development of cracking associated with the compressive ring. The NTU studies provided a good approximation for the large deflection criterion by suggesting that TMA takes place upon the deflection reaching the same level as the thickness of the slab. They were able to support this criterion by considering the lateral deflection of the columns, which more clearly demonstrated the tensile forces and 'pulling-in' of the slab [40–42]. Indeed, a clear definition of tensile membrane action ought to consider the tractions within the slab and their magnitude and use that information to assess both initiation of TMA and its diminishment followed by collapse. While the cracking associated with the compressive ring was clear in single-panel tests under uniform boundary conditions, it was less obvious for corner panels (Fig. 20 (a), (c), and (d)) and for slabs with intermediate beams (Fig. 10 (a) and (b)).

6.2. Recommendations for Structural Fire Resistance Design

The body of literature reviewed in this paper has highlighted a few important aspects of the behaviour of composite floors in fire that ought to be considered in design. While more research is still needed to better understand the development of TMA as noted earlier, the following points stand out based on current observations and understanding.

6.2.1. Reinforcement bar splicing and detailing

Additional reinforcement bars were spread over the hogging regions within the Shandong Jianzhu University experimental building. Despite severe cracking across multiple panels, reinforcement fracture was not observed [45–47]. While the Shandong Jianzhu University tests were performed on flat slabs without steel decking, this practice ought to be maintained in more traditional composite construction where only an anti-cracking mesh is used. This would prevent the potential failure by reinforcement fracture at the support which was highlighted by the NTU experiments as one of the governing failure conditions for their tests [40–42].

Furthermore, splicing of reinforcement bars and reinforcement meshes is essential for sustaining TMA. The continuity of the reinforcement mesh, ensured by adequate lap splicing, provides a path for the tensile tractions to flow and prevents large cracks from taking place. Incorrect lap splicing may result in large through-depth cracks as observed in the corner panel from Yang et al. [46]. When fire safety is a priority, additional quality assurance measures must be put in place to ensure that detailing requirements are met. Additional reinforcement bars at high-restraint edges and corners can also provide additional anchoring points for TMA thus giving it additional load paths to develop its full capacity.

6.2.2. Edge beams are critical for fire resistance

Edge beams are a critical component for the fire resistance of composite slabs. These beams provide the necessary support for TMA to develop if the reinforcement mesh can withstand the ultimate tensile tractions and the concrete could handle the compressive stresses. It was shown by Nguyen and Tan [61] that the actual flexibility and deformation of edge beams can reduce the overall capacity predicted by the yield line theory. It was also noted by Usmani and Cameron [78] that edge beams must be designed with sufficient anchoring capacity to allow for the reserve capacity of slabs in fire to fully manifest. It is thus essential that edge beams are properly fire protected. It was indeed noted in COSSFIRE that faulty fire protection of an edge beam resulted in its premature failure [17].

6.2.3. Smart application of fire protection

Some studies suggest that protection could be withheld from some internal secondary beams by relying on TMA to resist loads at elevated temperatures [25]. Wang and Dong [45] even suggest that it may be feasible to leave all floor framing and connections uninsulated as long as columns are fully protected. Others however, such as Wellman et al. [21], recommend performing additional analysis and testing before considering leaving any internal beams unprotected. Furthermore, most connections that were tested as part of the various system-level experiments demonstrated robust behaviour and none instigated uncontrolled failure regardless of the level of fire protection.

These findings point that different structures require varying degrees of fire protection to sustain fire exposure safely. For a performance-based approach, designers ought to rely on detailed analyses and testing that would ascertain their structural assemblies would meet the necessary performance criteria. Whether this means withholding fire protection from internal secondary floor beams or applying protection to every member is highly dependent on the structure and performance criteria. There is simply no one-size-fits-all solution and detailed analysis or testing are recommended for bespoke and highly irregular structural assemblies.

6.2.4. Design for utilising TMA capacity

There are several design methods for composite floors in fire. As noted in this paper, each of these methods has shortcomings and none have been presented as meeting the code-specified level of safety [79]. Most of these methods rely on simplifying assumptions that may result in unconservative capacity estimates, such as the assumption of rigid edge beams when using the yield line theory which was corrected for by Nguyen and Tan [61]. Additionally, most experimental work reviewed in this paper was performed on idealized and often scaled assemblies, and thus may not be representative of more complex structures. Therefore, while the methods discussed here may be suitable for initial estimates during preliminary design, it is difficult to recommend with confidence a single method for detailed design for all situations. It is best for designers to practice good engineering judgement when using their method of choice and verify their findings against numerical models and experimental testing.

7. Conclusions

A wealth of experimental data has been generated on the behaviour of composite floors in fire over the last two decades. Intrigued by the effect of large deflections on load carrying capacity, early tests on isolated slabs were performed at ambient conditions and induced these deflection levels by increasing the applied load. At ambient conditions, large deflections induce yield-line cracking in isolated slabs which paved the way for yield line approaches. Despite yield-line cracks not consistently manifesting in thermally loaded tests, the yield line method persisted as its predictions seemed to correspond well with observed slab capacities.

In addition to tests on isolated specimens, several tests were performed on composite floor assemblies in which the steel floor framing is composite with the slab. Mostly performed at elevated temperatures, these tests showed that edge boundary conditions, be it in vertical support or torsional restraint, are critical for the performance of composite floors. These tests also showed that yield-line cracks do not really form under fire conditions when the floor slab is supported and restrained not only on the edges but also across the span. The effect of continuity of such an arrangement was then made apparent by tests performed on full-sized structures.

Despite the tremendous efforts the community has put into studying the behaviour of composite floors in fire and the many valuable findings collected, there remains multiple avenues for future research. Previous studies have shown that there is a need for studying the effect of moderate fires, slab continuity, finite edge restraint, and the potential effect steel decking may have on the fire resistance. Furthermore, it is important to establish new criteria for failure, considering that almost all tests exceeded the current displacement criteria without becoming structurally unstable. Practitioners, on the other hand, ought to ensure adequate detailing, sufficient protection for edge beams, and always accompany decisions to withhold fire protection with detailed numerical analysis.

Acknowledgements

This work was supported by the Hong Kong Research Grants Council General Research Fund (No. 15220618), Theme-based Research Scheme (No. T22-505/19-N), and The Hong Kong Polytechnic University start-up fund (Project No. P0031564). M.A.O thanks the support from the Hong Kong PhD Fellowship Scheme.

References

1. BSI (2004) BS EN 1994-1-1 - Eurocode 4. Design of composite steel and concrete structures. General rules and rules for buildings
2. Shen M hui, Chung KF, Elghazouli AY, Tong JZ (2020) Structural behaviour of stud shear connections in composite floors with various connector arrangements and profiled deck configurations. Eng Struct 210:. https://doi.org/10.1016/j.engstruct.2020.110370
3. Izzuddin BA, Moore DB (2002) Lessons from a full-scale fire test. Proc Inst Civ Eng Struct Build 152:319–329. https://doi.org/10.1680/stbu.2002.152.4.319
4. British Steel (1997) The Behavior Of Multi Storey Steel Framed Buildings In Fire
5. The Steel Construction Institute (1991) Structural fire engineering investigation of Broadgate phase 8 fire
6. Bailey CG (2003) Efficient arrangement of reinforcement for membrane behaviour of composite floor slabs in fire conditions. J Constr Steel Res 59:931–949. https://doi.org/10.1016/S0143-974X(02)00116-5
7. Jiang J, Khazaeinejad P, Usmani A (2012) Nonlinear analysis of shell structures in fire using OpenSees
8. Usmani AS, Rotter JM, Lamont S, et al (2001) Fundamental principles of structural behaviour under thermal effects. Fire Saf J 36:721–744. https://doi.org/10.1016/S0379-7112(01)00037-6
9. Orabi MA, Jiang L, Usmani A, Torero J (2020) The Collapse of World Trade Center 7: Revisited. In: The 11th International Conference on Structures in Fire (SIF2020). pp 23–33
10. Orabi MA, Jiang L, Usmani A, Torero J (2022) The Collapse of World Trade Center 7: Revisited. Fire Technol. https://doi.org/10.1007/s10694-022-01225-2
11. Lawson RM (2001) Fire engineering design of steel and composite buildings. J Constr Steel Res 57:1233–1247. https://doi.org/10.1016/S0143-974X(01)00051-7
12. Plank RJ (2000) The performance of composite 8 steel-framed building. 179–186
13. Wang YC (2005) Performance of steel-concrete composite structures in fire. Prog Struct Eng Mater 7:86–102. https://doi.org/10.1002/pse.197
14. Wellman E, Varma AH, Fike R, Kodur V (2010) Experimental evaluation of composite floor assemblies under fire loading. Struct Congr 2010 1310–1319. https://doi.org/10.1061/41130(369)119
15. Fike R, Kodur V (2011) Enhancing the fire resistance of composite floor assemblies through the use of steel fiber reinforced concrete. Eng Struct 33:2870–2878. https://doi.org/10.1016/j.engstruct.2011.06.011
16. Vassart O, Zhao B (2011) FRACOF: Fire Resistance Assessment of Partially Protected Composite Floors - Engineering Background
17. Zhao B, Roosefid M, Breunese A, et al (2011) COSSFIRE: Final Report
18. Foster SJ (2006) Tensile Membrane Action of Reinforced Concrete Slabs at Ambient and Elevated Temperatures. PhD

19. Abu AK (2008) Behaviour of Composite Floor Systems in Fire. 204
20. Li G-Q, Zhang N, Jiang J (2017) Experimental investigation on thermal and mechanical behaviour of composite floors exposed to standard fire. Fire Saf J 89:63–76. https://doi.org/https://doi.org/10.1016/j.firesaf.2017.02.009
21. Wellman EI, Varma AH, Fike R, Kodur V (2011) Experimental evaluation of thin composite floor assemblies under fire loading. J Struct Eng 137:1002–1016. https://doi.org/10.1061/(ASCE)ST.1943-541X.0000451
22. Bailey CG, Moore DB (2000) The structural behaviour of steel frames with composite floorslabs subject to fire: Part 2: Design. Struct Eng 78:28–33
23. Lim L, Wade C (2002) Experimental Fire Tests of Two-Way Concrete Slabs. New Zealand
24. Lim L, Buchanan A, Moss P, Franssen J (2004) Numerical modelling of two-way reinforced concrete slabs in fire. Eng Struct 26:1081–1091. https://doi.org/10.1016/j.engstruct.2004.03.009
25. Bailey CG, Toh WS (2007) Behaviour of concrete floor slabs at ambient and elevated temperatures. Fire Saf J 42:425–436. https://doi.org/10.1016/j.firesaf.2006.11.009
26. Foster SJ, Bailey CG, Burgess IW, Plank RJ (2004) Experimental behaviour of concrete floor slabs at large displacements. Eng Struct 26:1231–1247. https://doi.org/10.1016/j.engstruct.2004.04.002
27. Cashell KA, Elghazouli AY, Izzuddin BA (2011) Failure assessment of lightly reinforced floor slabs. I: Experimental investigation. J Struct Eng 137:977–988. https://doi.org/10.1061/(ASCE)ST.1943-541X.0000420
28. Cashell KA (2009) Ultimate behaviour of floor slabs under extreme loading conditions. Imperial College London
29. Cashell KA, Elghazouli AY, Izzuddin BA (2011) Failure assessment of lightly reinforced floor slabs. II: Analytical studies. J Struct Eng 137:989–1001. https://doi.org/10.1061/(ASCE)ST.1943-541X.0000445
30. Florides MM, Cashell KA (2017) Numerical Modelling of Composite Floor Slabs Subject to Large Deflections. Structures 9:112–122. https://doi.org/10.1016/j.istruc.2016.10.003
31. Cashell KA, Elghazouli AY, Izzuddin BA (2010) Ultimate behavior of idealized composite floor elements at ambient and elevated temperature. Fire Technol. 46:67–89
32. Fan S, Sun W, Wei H, Liu M (2015) Research on the membrane action of profiled steel sheet-concrete composite floors in fire. Adv Steel Constr 11:469–491. https://doi.org/10.18057/IJASC.2015.11.4.5
33. Bailey CG, White DS, Moore DB (2000) The tensile membrane action of unrestrained composite slabs simulated under fire conditions. Eng. Struct. 22:1583–1595
34. Rezaeian H, Clifton GC, Lim JBP (2020) Failure modes for composite steel deck diaphragms subjected to in-plane shear forces – A review. Eng Fail Anal 107:104199. https://doi.org/10.1016/j.engfailanal.2019.104199
35. Vassart O, Zhao B (2012) MACS+: Engineering Background
36. BSi (2005) EN 1993-1-8:2005 Design of Steel Structures - Part 1-8: Design of joints
37. BSi (2005) EN 1991-1-1:2005 Eurocode 1: Actions on structures
38. Zhao B, Roosefid M (2011) Experimental and numerical investigations of steel and concrete composite floors subjected to ISO fire condition. J Struct Fire Eng 2:301–310. https://doi.org/10.1260/2040-2317.2.4.301
39. Bisby L, Gales J, Maluk C (2013) A contemporary review of large-scale non-standard structural fire testing. Fire Sci Rev 2:1. https://doi.org/10.1186/2193-0414-2-1
40. Tan KH, Nguyen TT (2015) Experimental and numerical evaluation of composite floor systems

under fire conditions. J Constr Steel Res 105:86–96. https://doi.org/10.1016/j.jcsr.2014.11.002
41. Nguyen TT, Tan KH (2017) Behaviour of composite floors with different sizes of edge beams in fire. J Constr Steel Res 129:28–41. https://doi.org/10.1016/j.jcsr.2016.10.018
42. Nguyen TT, Tan KH, Burgess IW (2015) Behaviour of composite slab-beam systems at elevated temperatures: Experimental and numerical investigation. Eng Struct 82:199–213. https://doi.org/10.1016/j.engstruct.2014.10.044
43. Tan K, Nguyen T (2015) Experimental and numerical evaluation of composite fl oor systems under fire conditions. J Constr Steel Res 105:86–96. https://doi.org/10.1016/j.jcsr.2014.11.002
44. Zhao B, Kruppa J (2004) Structural behaviour of an open car park under real fire scenarios. Fire Mater 28:269–280. https://doi.org/10.1002/fam.867
45. Wang Y, Dong YL, Li B, Zhou GC (2013) A fire test on continuous reinforced concrete slabs in a full-scale multi-story steel-framed building. Fire Saf J 61:232–242. https://doi.org/10.1016/j.firesaf.2013.08.005
46. Yang ZN, Dong YL, Xu WJ (2013) Fire tests on two-way concrete slabs in a full-scale multi-storey steel-framed building. Fire Saf J 58:38–48. https://doi.org/10.1016/j.firesaf.2013.01.023
47. Li B, Dong YL, Zhang DS (2015) Fire behaviour of continuous reinforced concrete slabs in a full-scale multi-storey steel-framed building. Fire Saf J 71:226–237. https://doi.org/10.1016/j.firesaf.2014.11.021
48. Usmani AS, Cameron NJK (2004) Limit capacity of laterally restrained reinforced concrete floor slabs in fire. Cem Concr Compos 26:127–140. https://doi.org/10.1016/S0958-9465(03)00090-8
49. Johansen KW (1943) Brudlinieteorier. I kommission hos J. Gjellerup
50. Hognestad E (1953) Yield-line theory for the ultimate flexural strength of reinforced concrete slabs. In: ACI Journal. pp 637–656
51. Kemp KO (1967) Yield of a square reinforced concrete slab on simple supports, allowing for membrane forces. Struct Eng 45:235–240
52. Hayes B (1968) Allowing for membrane action in the plastic analysis of rectangular reinforced concrete slabs. Mag Concr Res 20:205–212. https://doi.org/10.1680/macr.1968.20.65.205
53. Hayes B (1968) Study of the design of reinforced concrete slabs. University of Manchester
54. Burgess I (2017) Yield-line plasticity and tensile membrane action in lightly-reinforced rectangular concrete slabs. Eng Struct 138:195–214. https://doi.org/10.1016/j.engstruct.2017.01.072
55. Bailey CG (2001) Membrane action of unrestrained lightly reinforced concrete slabs at large displacements. Eng Struct 23:470–483. https://doi.org/10.1016/S0141-0296(00)00064-X
56. Bailey CG, Moore DB (2000) The structural behaviour of steel frames with composite floorslabs subject to fire: Part 1: Theory. Struct Eng 78:19–27
57. Bailey CG, Moore DB (2000) The structural behaviour of steel frames with composite floorslabs subject to fire: Part 2: Design. Struct Eng 78:28–33
58. Bailey CG, Toh WS, Chan BM (2008) Simplified and advanced analysis of membrane action of concrete slabs. ACI Struct J 105:30–40. https://doi.org/10.14359/19066
59. Clifton C, Hinderhofer M, Schmid R (2001) Design of multi-storey steel framed buildings with unprotected secondary beams or joists for dependable inelastic response in severe fires. HERA, Manukau City, New Zealand
60. Clifton C (2006) Design of composite steel floor systems for severe fires. Manukau City, New Zealand
61. Nguyen TT, Tan KH (2015) Ultimate load of composite floors in fire with flexible supporting edge beams. J Constr Steel Res 109:47–60. https://doi.org/10.1016/j.jcsr.2015.03.004

62. Burgess I, Chan B (2020) An integrated yield-line approach to tensile and compressive membrane actions in thin lightly-reinforced concrete slabs. Eng. Struct. 208
63. Cameron NJK, Usmani AS (2005) A new design method to determine the membrane capacity of laterally restrained composite floor slabs in fire Part 2: Validation. Struct Eng 83:34–39
64. Omer E, Izzuddin BA, Elghazouli AY (2010) Failure of unrestrained lightly reinforced concrete slabs under fire, Part I: Analytical models. Eng Struct 32:2631–2646. https://doi.org/10.1016/j.engstruct.2010.04.039
65. Omer E, Izzuddin BA, Elghazouli AY (2010) Failure of unrestrained lightly reinforced concrete slabs under fire, Part II: Verification and application. Eng Struct 32:2647–2657. https://doi.org/10.1016/j.engstruct.2010.04.035
66. Omer E, Izzuddin BA, Elghazouli AY (2009) Failure of Lightly Reinforced Concrete Floor Slabs with Planar Edge Restraints under Fire. J Struct Eng 135:1068–1080. https://doi.org/10.1061/_ASCE_0733-9445_2009_135:9_1068
67. Burgess I (2017) Yield-line plasticity and tensile membrane action in lightly-reinforced rectangular concrete slabs. Eng Struct 138:195–214. https://doi.org/10.1016/j.engstruct.2017.01.072
68. Burgess I, Sahin M (2018) Tensile Membrane Action of Lightly-reinforced Rectangular Composite Slabs in Fire. Structures 16:176–197. https://doi.org/10.1016/j.istruc.2018.09.011
69. Cameron NJK, Usmani AS (2005) New design method to determine the membrane capacity of laterally restrained composite floor slabs in fire Part 1 : Theory and method. Struct Eng 83:28–33
70. Gillie M, Usmani A, Rotter M, O'Connor M (2001) Modelling of heated composite floor slabs with reference to the Cardington experiments. Fire Saf J 36:745–767. https://doi.org/10.1016/S0379-7112(01)00038-8
71. Lamont S, Usmani AS, Gillie M (2004) Behaviour of a small composite steel frame structure in a "long-cool" and a "short-hot" fire. Fire Saf J 39:327–357. https://doi.org/10.1016/j.firesaf.2004.01.002
72. Sanad AM, Lamont S, Usmani AS, Rotter JM (2000) Structural behaviour in fire compartment under different heating regimes — Part 1 (slab thermal gradients). Fire Saf J 35:99–116. https://doi.org/10.1016/S0379-7112(00)00024-2
73. BSi (2004) Eurocode 2: Design of concrete structures - General rules - Structural fire design
74. Abu AK, Burgess IW, Plank RJ (2013) Tensile membrane action of thin slabs exposed to thermal gradients. J Eng Mech 139:1497–1507. https://doi.org/10.1061/(ASCE)EM.1943-7889.0000597
75. Li GQ, Guo SX, Zhou HS (2007) Modeling of membrane action in floor slabs subjected to fire. Eng Struct 29:880–887. https://doi.org/10.1016/j.engstruct.2006.06.025
76. Zhang NS, Li GQ (2010) A new method to analyze the membrane action of composite floor slabs in fire condition. Fire Technol 46:3–18. https://doi.org/10.1007/s10694-009-0086-8
77. Garlock M, Paya-Zaforteza I, Kodur V, Gu L (2012) Fire hazard in bridges: Review, assessment and repair strategies. Eng Struct 35:89–98. https://doi.org/10.1016/j.engstruct.2011.11.002
78. Usmani AS, Cameron NJK (2004) Limit capacity of laterally restrained reinforced concrete floor slabs in fire. Cem Concr Compos 26:127–140
79. BSi (2002) EN 1990 Eurocode 0: Basis for structural design